Mechanisms Controlling the Diurnal Solar Tide: Analysis Using a GCM and a Linear Model

U. Achatz,[1,2] N. Grieger,[1] and H. Schmidt,[3]

U. Achatz, Institut für Atmosphäre und Umwelt, Johann Wolfgang Goethe-Universität Frankfurt am Main, Altenhöferallee 1, 60438 Frankfurt am Main, (achatz@iau.uni-frankfurt.de)

N. Grieger, Leibniz-Institut für Atmosphärenphysik an der Universität Rostock, Schloßstr. 6, 18225 Kühlungsborn, Germany (grieger@iap-kborn.de)

H. Schmidt, Max-Planck-Institut für Meteorologie, Bundesstr. 53, 20146 Hamburg, Germany (hauke.schmidt@dkrz.de)

[1]Leibniz-Institut für Atmosphärenphysik
an der Universität Rostock, Kühlungsborn,
Germany.

[2]now at Institut für Atmosphäre und
Umwelt, Johann Wolfgang
Goethe-Universität, Frankfurt am Main,
Germany.

[3]Max-Planck-Institut für Meteorologie,
Hamburg, Germany.

Abstract. A GCM (HAMMONIA) and a linear model are used for analyzing the dynamics of the total diurnal solar tide in the mesosphere and lower thermosphere, comprising both the migrating and all nonmigrating components. A comparison between this tide in the GCM and in published observations is relatively favorable. The linear model uses monthly means from the GCM as background atmosphere and the diurnal heating rates from that model as forcing. The background atmosphere may be longitude-dependent, so that stationary planetary waves can be included. A straightforward analysis of corresponding effects is thus facilitated. To a large degree the seasonal variability of the diurnal tide is due to variations in the background atmosphere. In addition to corresponding previous results on the impact of the zonal-mean atmosphere on the migrating tide the thermospheric tide is shown to be strongly influenced by the variability of the absorption of solar radiation by O_2. With regard to the nonmigrating tidal components, their most important forcing mechanisms are tropospheric, as for the migrating tide below the thermosphere, and their seasonal cycle is mostly controlled by variations of the background atmosphere. In the dynamics of these components, however, the planetary waves take an active role. They can cause reductions in the tidal amplitude, by destructive interference with the directly forced nonmigrating tide, as for DS0 in February. The opposite effect of enhancing the tidal amplitude is also observed, in DW2 in the same season. The component DE3 is controlled by an interplay between the variability of the zonal-mean background and the diurnal heating. The correct simulation of

a meridional-wind-amplitude minimum in this tide during May — August seems to depend critically on the phase relation between the two.

1. Introduction

The diurnal cycle of solar heating leads to a dynamic response of the atmosphere which can be characterized as forced, horizontally and vertically propagating, large-scale waves in both temperature and winds. Especially in the mesosphere, the amplitude of these solar tides is so large that they represent a major component of atmospheric variability. The solar heating happens mostly in the troposphere, via the absorption of incoming radiation by water vapor and by latent heat release. A secondary role is played by the absorption of solar radiation by stratospheric ozone. In addition, solar tides are modulated sensitively by the propagation conditions they encounter between the forcing region and the mesosphere/lower thermosphere (MLT). Via their dynamical fields they also influence the upward propagation of smaller-scale gravity waves which are responsible for driving the global circulation in the middle atmosphere. They are therefore an important element of the coupling between the MLT and the atmospheric layers below. One may expect that many aspects of variability in the troposphere and stratosphere are communicated to the MLT by solar tides. A detailed understanding of the mechanisms controlling the forcing and propagation of solar tides is therefore a prerequisite to understanding climate trends and variability in this height region.

At night, solar heating is switched off completely. The time dependence of solar tides is therefore not a harmonic oscillation with a 24h period, but must be described as a superposition of tidal components oscillating at this period and its subharmonics. Likewise, the emitting altitude range is not zonally symmetric, so that a rather complex spatial dependence arises. In general, the spatial and time dependence of the signature of the

solar tides in any dynamic variable X is given by

$$X(\lambda,\phi,z,t) = \sum_{n=1}^{\infty}\{ \quad A_{n,0}(\phi,z)\cos\left(n\Omega t - \Phi^{e}_{n,0}\right) + \sum_{s=1}^{\infty}\left[A^{e}_{n,s}(\phi,z)\cos\left(n\Omega t - s\lambda - \Phi^{e}_{n,s}\right) + A^{w}_{n,s}(\phi,z)\cos\left(n\Omega t + s\lambda - \Phi^{w}_{n,s}\right)\right]\Big\} \quad . \tag{1}$$

Here λ and ϕ denote the geographic longitude and latitude, respectively. The altitude is given by z, and t is the universal time. The rotation rate of the earth is $\Omega = 2\pi/24\text{h}$. The temporal subharmonics corresponding to $n = 1, 2, 3$ are the diurnal, semidiurnal, and terdiurnal tide, respectively. Each is decomposed into a zonally symmetric part, with zonal wave number $s = 0$, and east- and westward travelling components at zonal wave numbers $s > 0$ with amplitudes $A^{e}_{n,s}$ and $A^{w}_{n,s}$, and phases $\Phi^{e}_{n,s}$ and $\Phi^{w}_{n,s}$, respectively. The diurnal tide is the focus of this study. For conciseness, a westward or eastward travelling component at wave number s will be called DWs or DEs, respectively. The name for the corresponding zonally symmetric component is DS0.

The apparent movement of the sun around the globe is westward. A leading tidal component of each temporal subharmonic is therefore the westward travelling one at wave number $s = n$, called the migrating tide. Its movement is synchronous to that of the sun. Historically, it was the migrating tides which first attracted most of the scientific interest, with the traditional source of information being surface pressure variations [*Chapman and Lindzen*, 1970]. Even more recently they have been studied using ground-based measurements [*Chang and Avery*, 1997; *Manson et al.*, 1999; *Tsuda et al.*, 1999, e.g.] or satellites [*Hitchman and Leovy*, 1985; *Dudhia et al.*, 1993; *Burrage et al.*, 1995; *McLandress et al.*, 1996; *Khattatov et al.*, 1997; *Wu et al.*, 1998; *Shepherd et al.*, 1999; *Oberheide et al.*,

2000; *Huang and Reber*, 2003; *Zhang and Shepherd*, 2005; *Forbes et al.*, 2006; *Huang et al.*, 2006; *Wu et al.*, 2006; *Zhu et al.*, 2006, e.g.]. The diurnal migrating tide is thought to be mainly forced by the direct absorption of solar radiation by tropospheric water vapor and stratospheric ozone. Corresponding model studies have been performed, e.g., by *Forbes* [1982]; *Vial and Forbes* [1989]; *Hagan et al.* [1995]; *Akmaev et al.* [1996]; *Hagan et al.* [2001]; *McLandress* [2002a, b].

All the other components are summarized under the class of nonmigrating tides. These can travel either westward or eastward, or remain standing ($s = 0$). Early observational studies of nonmigrating tides are the ones by *Wallace and Tadd* [1974], using rawinsonde data for the troposphere and stratosphere, and *Yagai* [1989], who derived nonmigrating tidal signatures from surface pressure data. However, it was not before the advent of global satellite measurements of winds and temperature in the middle atmosphere that it became possible to well discriminate between the migrating and nonmigrating tides in the mesosphere [*Lieberman*, 1991; *Talaat and Lieberman*, 1999; *Luo and Meek*, 2002; *Manson et al.*, 2004; *Oberheide and Gusev*, 2002; *Forbes et al.*, 2003; *Huang and Reber*, 2004; *Forbes et al.*, 2006; *Forbes and Wu*, 2006; *Oberheide et al.*, 2006; *Zhang et al.*, 2006]. It turns out that especially at low latitudes the nonmigrating contribution to the total tide can be substantial. The mechanisms by which nonmigrating tides are produced have been subject of various model studies [*Hamilton*, 1981; *Kato et al.*, 1982; *Forbes and Groves*, 1987; *Tsuda and Kato*, 1989; *Lieberman and Leovy*, 1995; *Ekanayake et al.*, 1997; *Hagan et al.*, 1997; *Miyahara et al.*, 1999; *Grieger et al.*, 2002; *Hagan and Forbes*, 2002, e.g.]. One of the important mechanisms emerging is the direct forcing of nonmigrating tides by the nonmigrating component of latent heat release. This is thought to be the most

relevant mechanism for the component DE3. Another one, however, is the modulation of tides, produced by the migrating forcing in the troposphere, by stationary planetary waves in the stratosphere. *Hagan and Roble* [2001] have studied this process with the help of the Thermosphere Ionosphere Mesosphere Electrodynamics General Circulation Model (TIME-GCM). A migrating diurnal tide was prescribed at the lower boundary of the GCM (altitude 30km), as derived from a linear model with zonally symmetric background. The GCM was then integrated with prescribed planetary wave activity at the lower boundary. The mesospheric tide simulated by this model had significant nonmigrating components, most notably DS0 and DW2. A more direct approach to this problem is the one taken by *Grieger et al.* [2004], who used a linear model with a background atmosphere including planetary waves. They also find a significant impact from the interaction between migrating forcing and planetary waves. Indeed, *Lieberman et al.* [2004] report a clear correlation between the planetary wave activity and DW2 and DS0 in satellite data for the lower-mesospheric temperature.

An aspect of tidal variability attracting much attention is the seasonal cycle. The MLT amplitude of the migrating diurnal tide exhibits a strong semiannual variation with maxima at equinox and minima at solstice. This is observed both by ground-based radar [*Vincent et al.*, 1988, 1998; *Fritts and Isler*, 1994; *Manson et al.*, 2004], and on a global basis from satellites [*Hays et al.*, 1994; *Burrage et al.*, 1995; *McLandress et al.*, 1996; *Huang and Reber*, 2003; *Forbes et al.*, 2006; *Forbes and Wu*, 2006; *Huang et al.*, 2006]. Model studies identify the seasonal variation of the zonal-mean winds in the middle atmosphere as the main cause for this behavior [*McLandress*, 2002a, b; *Zhu et al.*, 2006]. The amplitudes of the nonmigrating diurnal tides undergo seasonal cycles which have

semiannual contributions, but also exhibit a strong annual variation [*Forbes et al.*, 2003; *Huang and Reber*, 2004; *Manson et al.*, 2004; *Oberheide et al.*, 2005; *Forbes and Wu*, 2006; *Oberheide et al.*, 2006; *Zhang et al.*, 2006]. The mechanisms behind this seasonal behavior are less clear. *Oberheide et al.* [2005, 2006] follow a similar strategy to the one from *Hagan and Roble* [2001] in using a linear model (Global Scale Wave Model, GSWM) and the TIME-GCM for simulating the seasonal cycle of the most important diurnal nonmigrating tides. The linear model, which does not describe the impact of planetary waves, is reported to reproduce the seasonal cycle of DE3. This component therefore seems to be controlled by the background atmosphere and the nonmigrating forcing, which is due to latent heat release. An open question remaining here is which part both factors play in determining the seasonal cycle of DE3. In the same studies, both the linear model and the GCM, the latter again with a migrating tide and the planetary waves prescribed at the lower boundary, yield seasonally varying components DS0 and DW2. These therefore seem to be controlled by two processes, the interaction of migrating forcing and planetary waves, and the direct nonmigrating forcing in interaction with a varying zonal mean in the background atmosphere. Some uncertainties, however, also remain here. Firstly, the respective role of variations in the zonal-mean background and the nonmigrating forcing is not clarified within GSWM. Secondly, the TIME-GCM integrations are fully nonlinear; corresponding feedbacks are not excluded. It is therefore not possible to simply add the GSWM result to the one from the GCM so as to obtain the complete tidal signal.

A more conclusive picture could arise from a linear model with a background atmosphere incorporating the most important stationary planetary waves. Such analyses shall be reported here. The corresponding heat sources and background atmosphere are, how-

ever, not obtained from observations but from a state-of the art GCM (HAMMONIA) ranging from the ground into the thermosphere. The advantage of such an approach, as also followed by *McLandress* [2002a, b], is the self-consistent framework available for the various factors in play. It certainly necessitates, however, a detailed validation of the tides in the GCM. The purpose of this study therefore is fourfold: (1) A comparison of the tides in HAMMONIA with available observations, (2) a validation of the tides from the linear model, (3) documenting within this framework the mechanisms causing the migrating and nonmigrating diurnal tide in the mesosphere, and (4) analyzing the mechanisms responsible for the seasonal cycle of the most important diurnal tides. The paper is thus structured as follows: Section 2 gives a short description of the GCM and presents the diurnal tide in the model. The linear model and its tides are described in section 3. It is then used in section 4 for an analysis of the dynamics of the migrating diurnal tide. A corresponding analysis of the most important nonmigrating tidal components is given in section 5. The effect of a possible GCM deficiency, concerning the amplitude of planetary waves, on the results of this study is assessed in section 6. The manuscript is finally summarized and discussed in section 7.

2. HAMMONIA

2.1. The Model

The three-dimensional Hamburg Model of the Neutral and Ionized Atmosphere (HAMMONIA) is a state-of-the-art GCM that treats atmospheric dynamics, radiation and chemistry interactively. It is a spectral model with triangular truncation at wave number 31 (T31) and with 67 levels between the surface and $1.7 \cdot 10^{-7}$hPa ($\sim$ 250km). The dynamical core is identical to the one from the MAECHAM5 model [*Giorgetta et al.*, 2006; *Manzini*

158 *et al.*, 2006]. The model includes comprehensive descriptions of the energy budget, the
159 water cycle, land surface processes, and a full dynamic and radiative coupling with the
160 MOZART3 chemical module [*Kinnison et al.*, 2007]. On top of this it includes solar heat-
161 ing in the ultraviolet and extreme ultraviolet wavelength regime, a non-LTE radiative
162 scheme, energy and momentum deposition and eddy diffusion generated by gravity wave
163 breaking, vertical molecular diffusion and conduction, and a simple parameterization of
164 electromagnetic forces in the thermosphere (ion drag and Lorenz forces). A description
165 of the model, its climatology, and the simulation used in this study are given by *Schmidt*
166 *et al.* [2006].

2.2. The Diurnal Solar Tide in HAMMONIA

167 The model data used for the analysis are the fields for the zonal (i.e. west-east) and
168 meridional (south-north) wind, the temperature, and the diabatic heat sources from a
169 20-year integration under solar-minimum conditions, sampled every 3h. On each grid
170 point, with 48 equidistant longitudes (via interpolation from the model grid) and the 48
171 gaussian latitudes used by the model, and for each month a mean diurnal cycle has been
172 formed from the available $20 \times 30 = 600$ days. The tides at each grid point have then
173 been determined via a Fourier analysis in time, thus obtaining a signal for the periods
174 24h, 12h, and 8h, and the monthly mean. Following this, the global diurnal tide has been
175 decomposed into the various migrating and non-migrating components, according to (1).
176 In the following we discuss results at geometric altitudes. For the interpolation from the
177 model hybrid pressure levels to these altitudes we have used the geopotential heights from
178 the zonal-mean monthly-mean states. According to our analyses this is an appropriate
179 approach. The amplitudes of the geopotential fluctuations associated with the solar tides

and the stationary planetary waves are everywhere less than 1km or 200m, respectively (not shown).

The March low-latitude MLT amplitude and phase of the migrating diurnal tide in the temperature and meridional wind are shown in Fig. 1. The phases are illustrated via the local solar time, $t_L = t + \lambda/\Omega$, at which the respective maximum value is reached, i.e. $\Phi^w_{1,1}/\Omega$. These results are to be compared to corresponding observational analyses by *McLandress et al.* [1996], *Zhang et al.* [2006], and *Zhu et al.* [2006]. Note that the phases published by *McLandress et al.* [1996] are chosen to range between 0h and 24h, while ours vary between -12h and 12h. The amplitudes of the diurnal tide in the meridional wind are in reasonable agreement with the observations, both in the maximum values and in the location where these are attained. The same holds for the phase structure, with about the same vertical gradient, corresponding to a vertical wavelength of the tide near 20km. Also the lines of constant phase agree approximately with the observations. The temperature amplitudes are again in quite reasonable agreement with the observational analyses published by *Zhang et al.* [2006] and *Zhu et al.* [2006]. Also here the phase gradient is about right, while the lines of constant phase are 5-10km lower than shown by *Zhang et al.* [2006].

Fig. 2 shows the seasonal dependence of the low-latitude amplitude of the diurnal migrating tide in the temperature at the altitudes 55km and 86km, and in the meridional wind at 95km. Especially in the upper mesosphere one recognizes the well-known semiannual oscillation. Its agreement with the available observational results is quite good. The temperature amplitude at 55km is in good agreement with the analyses of MLS data by *Huang et al.* [2006], with an equatorial maximum of about 3K in March, and a somewhat

weaker maximum in September. SABER data analyzed by the same authors also show a similar behavior, however with a rather strong amplitude increase toward the southern subtropics. The latter is not reproduced by the model. The temperature amplitudes at 86km are in good agreement with the SABER data analyses shown by *Zhang et al.* [2006]. The equatorial maxima in March and September are reproduced, as well as the secondary maxima in the same months at $\pm 30^\circ$ latitude. The seasonal cycle of the meridional wind at 95km can be compared with the satellite data analyses (TIDI and HRDI) by *Huang et al.* [2006]. The differences between the model and the observational results are well within the range of observational differences. The latter might at least in part be due to an interannual variability averaged out by the model analysis.

As mentioned earlier, at least part of the nonmigrating diurnal tide is forced by nonmigrating components in the diurnal heating. As an example, the amplitudes of the nonmigrating diurnal components of the tropospheric diabatic heating in the model, averaged without mass weighting between 0.2km and 15.2km altitude, are shown for July in Fig. 3. *Forbes et al.* [2003] attribute such spectra to the modulation of the zonal wave one solar input by the orographic wave numbers 1 and 4 at low latitudes, resulting in diurnal heating components at DE3, DS0, DW2, and DW5. The amplitudes of the modelled July nonmigrating diurnal temperature tide components at 110km and 86km altitude can be seen in Fig. 4. In agreement with available observational analyses, and for reasons not analyzed here, the components DW3 and DW5 do not propagate significantly into the MLT. For 110km altitude *Forbes et al.* [2006] show the corresponding decomposition derived from August SABER data. There, DE3 turns out to be dominant. Indeed, the HAMMONIA fields in August (not shown) exhibit a similar behavior, with the DE3 am-

plitude above 14K, and two weaker maxima of DS0 of about 7K at $\pm 30^\circ$ latitude and another one of DW2 of 3K on the equator. The spectral distribution of the nonmigrating temperature tide at 86km can be compared to corresponding analyses of MLS data by *Forbes and Wu* [2006]. The agreement here is less good. While the observations indicate a dominant DW2 component of about 2-3K, the model has its strongest contribution from DE3 with somewhat above 3K. What the model is also missing is any significant extratropical contribution, while the observational analyses indicate quite strong activity of DW2 and DS0 in the southern extratropics.

The seasonal cycle of the amplitudes of various nonmigrating components in the model is shown in Fig. 5. Comparing this to the observational analyses of *Forbes et al.* [2003] and *Oberheide et al.* [2005, 2006] one finds quite good agreement with the DW2 component in the horizontal winds at 95km, especially the meridional wind. The horizontal wind signal of DE3 reproduces the maxima in February/March and November in the meridional wind, but misses the corresponding minimum in June — August. The zonal wind shows a maximum near August, as the observations, but unlike the observations there is no minimal activity in the other months. The temperature tides in Fig. 5 can be compared to analyses of SABER data by *Forbes et al.* [2006]. The agreement in DE3 is quite reasonable, with a prominent equatorial maximum in September. The model does, however, also produce a secondary maximum around January, which is not found in the observations. As for DW2, both the model and the observations maximize in November, but the latitudinal structure is not reproduced as well. The maximum of DS0 occurs in the model around June, while the observations rather place it around September.

Summarizing the comparisons in this section, the HAMMONIA model simulates the migrating diurnal tide in quite a realistic manner. This holds especially for the amplitudes, including their seasonal cycle. Among the nonmigrating diurnal tides, the same dominant components, DE3, DS0, and DW2, are found as in the observations. The seasonal cycle of DW2 is reproduced rather realistically in the horizontal winds, less in the temperature, that of DE3 matches the observations mostly in the temperature, but in parts also in the meridional wind. The model agrees less well with the observations in the seasonal behavior of DS0.

3. The Linear Model

3.1. Model Description

Mainly focussing in the following on those aspects of the diurnal solar tide in HAMMONIA which are at least roughly in agreement with the available observations, we use a linear model for analyzing its dynamics. This model is basically the same as used by *Grieger et al.* [2004]. Its algorithm is based on the one of KMCM (Kühlungsborn Mechanistic Circulation Model), the simplified GCM described by *Becker and Schmitz* [2002]. Via the automatic differentiation tool TAMC (Tangent Adjoint Model Compiler) of *Giering and Kaminski* [1998] the KMCM algorithm (without physics) has been linearized, yielding a linearization of the primitive equations about an arbitrary reference state. In the applications here the linear model uses as reference state any of the monthly mean states obtained from the HAMMONIA data. In comparison with all other linear tidal models we are aware of this is the only one which allows the reference state to be zonally asymmetric. Stationary planetary waves are thus included. The model discretization employs spherical harmonics in the horizontal, with a triangular spectral resolution of T14.

In the vertical, 60 levels on a hybrid pressure coordinate are used between the ground and approximately 140km altitude. The level distribution can be deduced from Fig. 6. The tides are obtained by forcing the model with the diurnal cycle of the HAMMONIA diabatic heating. The model is, however, not integrated in time. Rather the model equations are Fourier transformed in time and the resulting set of linear equations for the component at the diurnal frequency are solved by a preconditioned conjugate-gradient method. In the light of its history the the model has been given the name LIN-KMCM.

Contributing heat sources taken from HAMMONIA are absorption of incoming short-wave radiation, heating related to tropospheric condensation and convection, chemical heating, and heat sources related to the ion drag (Joule heating) and to the dissipation of gravity wave energy. The heating by outgoing long-wave radiation is parameterized here by a newtonian cooling (see below). Explicitly adding the corresponding heating, as diagnosed from HAMMONIA, did not change our results. Heating due to absorption of solar irradiance is subdivided into three spectral regions: wavelengths λ longer than 250nm, between 120 and 250nm, and shorter than 120nm. In the following, these bands will be called SW, SR, and EUV, respectively. While the first band is dominated by contributions from tropospheric water vapor and stratospheric ozone, heating in the second band (that includes in particular the Schumann-Runge bands and continuum) is mainly due to absorption by O_2 in the mesosphere and lower thermosphere, and the extreme UV part of the spectrum is absorbed by atomic and molecular oxygen and nitrogen in the thermosphere. The linear model can calculate the response to each of these heat sources separately, which finally add up to produce the total signal.

The model 'physics' is very simple. Newtonian cooling is used to capture some aspects of radiative damping (Fig. 6). As for the effects of gravity waves, experiments with the Rayleigh damping used by *Grieger et al.* [2004] showed that it was rather contaminating the phase structure of the simulated tides. We have therefore decided to replace it by an altitude dependent 4th-order horizontal diffusion, modified in a manner ensuring angular-momentum conservation [*Becker*, 2001]. The corresponding profile, shown in Fig. 6, was tuned so as to yield a reasonable amplitude of the migrating diurnal tide in the MLT. In addition to the horizontal diffusion a weak vertical diffusion of $1 \cdot 10^{-2}\mathrm{m}^2/\mathrm{s}$ is used. We suspect that the present handling of gravity-wave effects is a source of inaccuracy in the model. It has been shown that, in comparison with simple descriptions by Rayleigh friction, only an incorporation of the explicit interaction between gravity waves and tides is able to yield realistic vertical wavelengths for the latter [*Ortland*, 2005a, b; *Ortland and Alexander*, 2006]. On the other hand *McLandress* [2002a] found, in an analysis of a GCM using the same gravity-wave parameterization as here in HAMMONIA, the gravity-wave impact on the migrating diurnal tide to be rather weak. Nonetheless, corresponding model improvements are planned for the future. For the time being, a successful performance of the model with regard to specific aspects of tidal dynamics are taken as indications that these are not predominantly due to the gravity-wave tidal interaction.

3.2. The Diurnal Solar Tide in the Linear Model

As a first indication of the performance of the linear model in comparison with HAMMONIA we show in Fig. 7 the amplitudes and phases of the March migrating diurnal tide in temperature and meridional wind. This is to be compared to Fig. 1. One sees that the linear model reproduces the essential aspects. As expected one also notes, however, that

the vertical wavelength is longer than in HAMMONIA. This might be a direct effect of the insufficient description of the interaction between gravity waves and tides. The seasonal cycle of the migrating diurnal tide in the linear model is shown in Fig. 8. The comparison with the behavior of HAMMONIA (Fig. 2) is quite favorable. As already discussed by *McLandress* [2002a], gravity waves seem not to be a major factor for the explanation of the semiannual oscillation of the migrating diurnal tide.

The linear model simulates the nonmigrating tides reasonably well. The spectral decomposition is similar to the GCM (not shown). Also in this model the components DE3, DS0, and DW2 dominate in the MLT. The seasonal cycles of their amplitudes are illustrated in Fig. 9. The agreement with the corresponding results from HAMMONIA (Fig. 5) is reasonable. It is interesting to note that there are even aspects which are simulated by the linear model with greater similarity to the observations than by HAMMONIA. This holds for the seasonal dependence of DE3 in the meridional wind, to be compared to the analyses by *Forbes et al.* [2003] and *Oberheide et al.* [2005, 2006]. DE3 in the linear model does not exhibit as clearly the June — August maximum in the meridional wind which is produced by HAMMONIA. It appears that some aspect of the intrinsically nonlinear dynamics of HAMMONIA might be causing problems in this regard.

4. Linear Dynamics of the Migrating Diurnal Tide

Having ensured the realism of the linear model with regard to simulations of the migrating diurnal tide, it shall be used here for a short analysis of the dominant mechanisms controlling its dynamics. We first look at which contributions of the diabatic heating are most relevant in causing the tide. The linear model can calculate the response to each of these heat sources separately, which finally add up to produce the total signal. Each of the

responses can also be decomposed directly into the part due to the respective migrating heating and the nonmigrating heat sources. The latter can contribute to the migrating tide by their interaction with the stationary waves in the background. The process behind this is a coupling, via the linear dynamics, between different zonal wavenumbers which is only possible in a longitude-dependent background. Fig. 10 shows the amplitude of the March response in the meridional-wind tide to the most important migrating heating rates. The nonmigrating components turn out to be among the minor factors (not shown). The dominant factor is the direct absorption of incoming solar radiation in the SW band (migrating part), which is itself dominated by the absorption by tropospheric water vapor. The stratospheric part of the SW-band absorption, presumably dominated by stratospheric ozone, plays a secondary role (not shown). Another relevant component is the absorption of radiation with shorter wavelengths (SR band). This effect is especially important in the thermosphere. Finally, also the heating by condensation and convection plays a non-negligible role. All remaining heat sources lead to amplitudes of less than 5m/s.

The same kind of decomposition for December is shown in Fig. 11. Seemingly the Schumann-Runge part plays a major role in the seasonal variability in the thermosphere. Near the mesopause, however, the background atmosphere is most important. This can be seen in Fig. 12. Here a seasonal cycle has been calculated in various ways. For discussing this let us note that the time dependent vector $\mathbf{X}(t)$ of spectral coefficients (of our spectral model) of the migrating diurnal tide in all dynamical fields (horizontal wind, temperature, and surface pressure) can be written as

$$\mathbf{X}(t) = \mathbf{C}\cos(\Omega t) + \mathbf{S}\sin(\Omega t) \quad , \tag{2}$$

and that the vector $\mathbf{Y} = (\mathbf{C}, \mathbf{S})$ of tidal coefficients satisfies in the linear model

$$\mathbf{Y}(m) = \mathcal{L}[\mathbf{X}_b(m)]\,\mathbf{F}(m) \qquad . \tag{3}$$

Here $\mathcal{L}$ is the tidal operator of the linear model, and $\mathbf{F}$ is the vector of tidal coefficients of the diurnal heat source. The former depends on the atmospheric background state $\mathbf{X}_b$. Both $\mathbf{F}$ and $\mathbf{X}_b$ depend on the month m. We now decompose the background state into its zonal mean $\overline{\mathbf{X}}_b$ and the stationary-wave part $\delta\mathbf{X}_b$. Similarly, the heating is decomposed into its annual mean $\langle\mathbf{F}\rangle$ and the seasonally varying part $\mathbf{f}(m)$. In a first calculation, as discussed above, we have used the linear model for calculating month-wise the full tidal signal, as given by (3). In a second calculation the yearly-mean heating has been taken and only the background state has been varied, i.e. we have determined $\mathcal{L}[\mathbf{X}_b(m)]\langle\mathbf{F}\rangle$. This indicates the contribution of variations in the atmospheric background state to the total seasonal cycle of the tide. The residual, i.e. the seasonal cycle in the tide due to seasonal variations in the forcing, is $\mathcal{L}[\mathbf{X}_b(m)]\,\mathbf{f}$. This component vanishes in the absence of a seasonal cycle in the forcing. Finally, in order to diagnose the contribution of the seasonal cycle in the stationary waves, they have been removed from the background, and the difference between the total signal and this calculation has been determined, i.e. $\left\{\mathcal{L}[\mathbf{X}_b(m)] - \mathcal{L}\left[\overline{\mathbf{X}}_b\right]\right\}\mathbf{F}(m)$. These results are shown in Fig. 12, using the amplitude of the meridional wind at 95km altitude. It is quite obvious that the seasonal cycle of the zonal mean of the atmospheric background state dominates the picture. Neither do the heat sources matter much nor does the seasonal cycle of the stationary planetary waves have a significant impact. This dominance of the zonal-mean tidal propagation conditions for the seasonal cycle of the migrating diurnal tide in the MLT further corroborates the corresponding findings from *McLandress* [2002a, b] and *Zhu et al.* [2006]. *McLandress*

371 [2002b] argues that the decisive factor in this behavior is the seasonal dependence of the
372 zonal-mean vorticity in the background atmosphere. This might also be the case here.
373 A more detailed analysis indicates that it is especially the propagation conditions below
374 70km altitude that matter (not shown).

5. The Non-Migrating Components

5.1. Dominant Forcing Mechanisms

375 It has been shown above that the linear model is roughly able to simulate the seasonal
376 cycle of the three most important nonmigrating components of the diurnal tide. The best
377 agreement with the available observations is certainly to be found for DW2, but also DS0
378 and DE3 reproduce aspects of the observed seasonal cycle. The latter holds specifically
379 for the meridional wind. Therefore we focus on this dynamical field in the discussion of
380 the dynamics of the nonmigrating diurnal tide.

381 For an identification of the major heat sources responsible for the occurrence of the
382 component DE3, Fig. 13 shows its meridional-wind amplitude in December, and the
383 amplitudes of the corresponding major contributions from the various heat sources. We
384 first note that the spatial dependence of the total amplitude is in reasonable agreement
385 with an observational analysis shown by *Oberheide et al.* [2006]. The tide is centered at the
386 equator with two maxima, one near 100km altitude, and the other one below. Our analysis
387 supports previous findings that DE3 is mostly forced by tropospheric latent heat release.
388 There is a secondary component due to the direct absorption of incoming short-wave solar
389 radiation. The migrating forcing does not produce a significant response. This indicates
390 that the modulation of the migrating tide by the longitude-dependent background, i.e.
391 the interaction between migrating tide and stationary waves, does not produce significant

392 contributions to DE3 in December, even though stratospheric planetary waves maximize
393 near that time of the year.

394 For an analysis of DS0 we show in Fig. 14 the corresponding fields for June, when
395 it is near to attaining its maximum amplitude near the mesopause. Again the June
396 result of *Oberheide et al.* [2006] is similar, in the sense that the maximum amplitude
397 at the mesopause is near 20°S. Even quantitatively the agreement is quite good. As
398 most important contributing factors we identify the absorption of incoming short-wave
399 solar radiation and condensation and convection. In contrast to DE3, in this case the
400 stationary planetary waves have an impact. The migrating forcing alone yields a weak
401 response in DS0 which can only be due to the modulation of a migrating tide in the lower
402 atmosphere by planetary waves. With regard to this factor we corroborate the results
403 from *Hagan and Roble* [2001] and *Oberheide et al.* [2005], however on a model basis which
404 is more straightforward than the one used by these authors and which excludes nonlinear
405 feedbacks. It might also be worth drawing the reader‘s attention to the fact that here, as
406 in many other cases, the amplitudes do not simply add up to yield the total. Differing
407 phases can lead to quite strong interference effects. Even more significant instances of
408 this kind of behavior follow below.

409 Finally we show the same type of analysis for DW2 in February in Fig. 15. Again the
410 amplitude of the total DW2 signal agrees quite well with the results of *Oberheide et al.*
411 [2006]. The decomposition reveals both condensation and convection and the migrating
412 forcing as the dominant contributors. Thus, the stationary planetary waves play an
413 important role in the dynamics of DW2, as already suggested by *Hagan and Roble* [2001].
414 The absorption of incoming solar radiation only has a minor impact.

5.2. Seasonal Cycle

We finally examine the dynamics of the seasonal cycle of the important nonmigrating components. This is done in exactly the same way as for the migrating tide above. Fig. 16 shows the corresponding results for DE3, once again using the amplitude in the meridional wind at 95km altitude. Clearly, the most important factor in controlling the seasonal cycle of DE3 is the seasonal variability in the zonal-mean background atmosphere. It would, however, produce a secondary maximum in August. One sees that it is the seasonal variability of the tidal forcing which acts against this, so that, as in the available observations, only the maximum between November an February remains, together with a weak secondary maximum in April. As was to be expected from the results above, the variability in the stationary planetary waves does not have an important effect. In the case of DS0, illustrated in Fig. 17, one finds again the variability of the zonal-mean background to be the major factor. It is interesting to note that even here the planetary waves do not leave many traces. They do have a quantitative impact (in December near 50% of the total signal), but clearly the zonal mean background dominates the scene. Fig. 18 finally shows the results for DW2. Again the zonal-mean background is most important. Here, however, the planetary waves positively act to enhance the seasonal cycle of the tide. This can be read from panel d) which shows the amplitude of the difference between the seasonal cycle in the full linear model and the corresponding result with zonal-mean background.

6. The effect of an increased planetary-wave activity

As shown above, planetary waves matter in the dynamics of the diurnal solar tide. One should, however, be aware that their effect is probably underestimated in the previous

sections. Fig. 19 shows a comparison between the seasonal cycle of the stationary planetary wave (monthly mean) at zonal wave number $s = 1$ in HAMMONIA and in ERA-40 reanalysis data at 50km altitude. One sees that especially in the horizontal wind the amplitude of the reanalysis data is stronger than in the model by about a factor 2. One might wonder what impact such a strong amplitude would have. Since the planetary wave in the temperature seems not to differ so much between model and analyses, we have chosen to double in the background state the planetary wave amplitude in the horizontal wind and leave that in the temperature as in HAMMONIA. With this new background the seasonal-cycle calculations with the linear model have been repeated. Additional calculations with twice the planetary-wave activity also in the temperature yield essentially the same results (not shown). The meridional-wind amplitudes at 95km in the migrating tide and the dominant nonmigrating components are seen in Fig. 20. Although only DW2 shows a significantly increased total amplitude, the planetary-wave part in the total signal is now considerably larger than before. It is interesting to note that at planetary-wave amplitudes closer to analysis data than in HAMMONIA even DE3 and the migrating diurnal tide seem to be influenced by the tidal modulation due to planetary waves. Clearly, this needs further validation by a GCM with a planetary-wave activity closer to the findings in analysis data, where then also the zonal-mean state would be dynamically consistent. At present, increasing the planetary-wave amplitudes only leads to a stronger impact from these waves onto the nonmigrating tides, but no improvement in the comparison with observations is found.

7. Summary and Discussion

457 The work reported here uses a combination of a GCM (HAMMONIA) and a linear
458 model for the exploration of the dynamics of solar tides. The GCM is taken as a source
459 of global data on the solar diurnal tides themselves, but also monthly mean states and
460 diabatic heat sources. The strengths of such an approach are the completeness of the
461 data set and its self-consistency. Data from observational analyses are usually limited in
462 altitude and latitude range, and with regard to the diabatic heat sources the available
463 information is most often rather indirect. The price one does pay in using GCM data is
464 that such a model is always just an approximation of real nature. A validation of the GCM
465 tides shows, however, that many important aspects of tidal observations are reproduced.
466 This holds most clearly for the migrating tide which shows a seasonal cycle which is
467 very close to the available observations. However, also numerous aspects of the observed
468 nonmigrating components are reproduced by the model. The same leading components
469 are found, and especially in the meridional wind several aspects of their seasonal cycle are
470 reproduced. This holds for DW2 and, with limitations, for DE3. The GCM has problems
471 in simulating the observed seasonal cycle of DS0.

472 The linear model is used for analyzing the seasonal behavior of the tides. A spe-
473 cial feature of the model, employing GCM monthly means as background atmosphere
474 and the diurnal heat sources from the same model as forcing, is its ability to handle a
475 longitude-dependent background. *Hagan and Roble* [2001] and *Oberheide et al.* [2005]
476 have examined the interaction between migrating forcing and stationary planetary waves
477 within the TIME-GCM. The linear model used here can add to their results by provid-
478 ing a linear framework within which nonlinear feedbacks are excluded, and the additive
479 effects of nonmigrating forcing and migrating forcing can be compared directly. This is

useful for assessing their comparative role both in the total tidal signal as such, and in its seasonal cycle. With regard to the migrating tide, the model corroborates the findings of others [*McLandress*, 2002a, b; *Zhu et al.*, 2006] that it is nearly exclusively the seasonal dependence of the zonal-mean background atmosphere which is responsible for the seasonal cycle of the tide near the mesopause. One can see this as a validation of the model, but a piece of information it adds is that in the lower thermosphere a directly thermospheric heating term turns out to be decisive for the seasonal cycle. This is the absorption of incoming solar radiation in the SR part of the spectrum from 120 to 250nm.

With regard to the nonmigrating tides, an interesting observation is that in comparison with observations the seasonal cycle of DE3 actually looks better in the linear model than in HAMMONIA. At the present state it cannot be excluded that this is an accident, but it might point at a deficiency in the nonlinear dynamics of HAMMONIA. One might e.g. speculate that the gravity-wave parameterization in the model is potentially too nonlinear in its behavior. This seems worthwhile further examinations in the future.

Anyway, the linear dynamics of the nonmigrating diurnal tides in the linear model has some interesting features. Perhaps least surprising is the important role played by condensation and convection in the forcing of DE3. An analysis of the seasonal cycle near the mesopause shows that the amplitude maximum between November and February is mostly due to an enhancing effect by the zonal-mean propagation conditions. An erroneous maximum in August in HAMMONIA is prevented in the linear model by a counteracting effect due to the seasonal cycle in the forcing. The interplay between the zonal-mean background and the forcing thus seems to be essential for explaining the complete seasonal cycle.

Around the time of its maximum (April — June) DS0 in the linear model is mostly due to the direct nonmigrating forcing by the absorption of short-wave solar radiation and by condensational heating. Since the planetary waves are weak during this time it is no surprise that their effect is not so important then. Indeed, it is found that most of the seasonal cycle can be understood as an effect of variations in the zonal-mean background. One might wonder why this even holds between December and February when the planetary waves are strong. A decomposition of the February DS0 tide into its components due to the major forcings in Fig. 21 exhibits an interesting behavior in this regard. The total signal is very similar to the direct nonmigrating input from condensation and convection. Nonetheless, both the effects from the direct nonmigrating forcing by the absorption of solar short-wave radiation and the modulation of the migrating forcing by the planetary waves are also strong. However, they obviously cancel each other. It thus seems that destructive interference effects such as here might also be an essential factor of the planetary-wave effect on nonmigrating tides.

An example where the planetary waves actually enhance the amplitude of a nonmigrating tide is DW2. This tidal component is driven to a large proportion by the nonmigrating forcing due to condensation and convection. The seasonal cycle can be explained to the largest part by the seasonal variations of the zonal-mean propagation conditions of this directly forced nonmigrating tide. One also has, however, a quantitatively important impact from the planetary-wave modulation of the migrating tide forced in the troposphere. This holds both for the total signal as such and for the simulated seasonal cycle.

In conclusion, planetary waves do seem to be a factor to be taken into account in the dynamics of solar tides. A linear model as used here in combination with a GCM is

helpful in quantifying their importance in comparison with the more classical processes of nonmigrating tides forced directly in a zonal-mean background atmosphere. One should be aware that the present analysis may actually underestimate this effect. Corresponding improvements should be on the agenda for the future. Preliminary results, show, however, that at realistic planetary-wave amplitudes even DW1 and DE3 are no longer unaffected by these waves. Another conclusion is that in many cases tidal variability is not due to variability of the sources (as is partially the case for DE3), but it is caused by the variability of the propagation conditions which the tides are exposed to in a varying background atmosphere. There are hints that solar variability can modify those too [*Kodera and Kuroda*, 2002; *Matthes et al.*, 2004], so that one might even speculate on a corresponding effect on solar tides in the MLT. Finally, one might wonder what exactly drives the partial control of the nonmigrating tides, in their seasonal cycle, by the zonal-mean background atmosphere. Analyses corresponding to the ones done by *McLandress* [2002b] for the migrating tide wcould help answering this question. Such are, however, beyond the scope of the present paper.

Acknowledgments. ECMWF ERA-40 data used in this study have been provided by ECMWF. This work is partially funded by the Deutsche Forschungsgemeinschaft (DFG) under the CAWSES SPP grant AC 72/2-1 (SOTIVAR).

References

Akmaev, R. A., J. M. Forbes, and M. E. Hagan (1996), Simulation of tides with a spectral mesosphere/lower thermosphere model, *Geophys. Res. Lett.*, *23*, 2173–2176.

546 Becker, E. (2001), Symmetric stress tensor formulation of horizontal momentum diffusion
547 in global models of atmospheric circulation, *J. Atmos. Sci.*, *58*, 269–282.

548 Becker, E., and G. Schmitz (2002), Energy deposition and turbulent dissipation owing to
549 gravity waves in the mesosphere, *J. Atmos. Sci.*, *59*, 54–68.

550 Burrage, M. D., M. E. Hagan, W. R. Skinner, D. L. Wu, and P. B. Hays (1995), Long-term
551 variability in the solar diurnal tide observed by HRDI and simulated by the GSWM,
552 *Geophys. Res. Lett.*, *22*, 2641–2644.

553 Chang, J. L., and S. K. Avery (1997), Observations of the diurnal tide in the mesosphere
554 and lower thermosphere over Christmas Island, *J. Geophys. Res.*, *102*, 1895–1907.

555 Chapman, S., and R. S. Lindzen (1970), *Atmospheric Tides*, D. Reidel, Dordrecht.

556 Dudhia, A., S. E. Smith, A. R. Wood, and F. W. Taylor (1993), Diurnal and semi-diurnal
557 temperature variability of the middle atmosphere as observed by ISAMS, *Geophys. Res.*
558 *Lett.*, *20*, 1251–1254.

559 Ekanayake, E. M. P., T. Aso, and S. Miyahara (1997), Background wind effect on prop-
560 agation of nonmigrating diurnal tides in the middle atmosphere, *J. Atmos. Sol.-Terr.*
561 *Phys.*, *59*, 401–429.

562 Forbes, J. M. (1982), Atmospheric tides. 1. Model description and results for the solar
563 diurnal component, *J. Geophys. Res.*, *87*, 5222–5240.

564 Forbes, J. M., and G. V. Groves (1987), Diurnal propagating tides in the low-latitude
565 middle atmosphere, *J. Atmos. Sol.-Terr. Phys.*, *49*, 153–164.

566 Forbes, J. M., and D. Wu (2006), Solar tides as revealed by measurements of mesosphere
567 temperature by the MLS experiment on UARS, *J. Atmos. Sci.*, *63*, 1776–1797.

568 Forbes, J. M., X. Zhang, E. R. Talaat, and W. Ward (2003), Nonmigrating diurnal tides
569 in the thermosphere, *J. Geophys. Res.*, *108*, 1033, doi:10.1029/2002JA009262.
570 Forbes, J. M., J. Russel, S. Miyahara, X. Zhang, S. Palo, M. Mlynczak, C. J. Mertens,
571 and M. E. Hagan (2006), Troposhere-thermosphere tidal coupling as measured by the
572 SABER instrument on TIMED during July-September 2002, *J. Geophys. Res.*, *111*,
573 A10S06, doi:10.1029/2005JA011492.
574 Fritts, D. C., and J. R. Isler (1994), Mean motion and tidal and two-day structure and
575 variability in the meososphere and lower thermosphere over Hawaii, *J. Atmios. Sci.*, *51*,
576 2145–2164.
577 Giering, R., and T. Kaminski (1998), Recipes for adjoint code construction, *ACM Trans.*
578 *Math. Software*, *24*(4), 437–474.
579 Giorgetta, M. A., E. Manzini, E. Roeckner, and L. Bengtsson (2006), Climatology and
580 forcing of the quasi-biennial oscillation in the MAECHAM5 model, *J. Climate*, *19*,
581 3882–3901.
582 Grieger, N., E. M. Volodin, G. Schmitz, P. Hoffmann, A. H. Manson, D. C. Fritts,
583 K. Igarashi, and W. Singer (2002), General circulation model results on migrating and
584 nonmigrating tides in the mesosphere and lower thermosphere. Part 1: Comparison
585 with observations, *J. Atmos. Sol.-Terr. Phys.*, *64*, 897–911.
586 Grieger, N., G. Schmitz, and U. Achatz (2004), The dependence of the nonmigrating
587 diurnal tide in the mesosphere and lower thermosphere on stationary planetary waves,
588 *J. Atmos. Sol.-Terr. Phys.*, *66*, 733–754.
589 Hagan, M. E., and J. M. Forbes (2002), Migrating and nonmigrating diurnal tides in the
590 middle and upper atmosphere excited by tropospheric latent heat release, *J. Geophys.*

Res., *107*, 4754, doi:10.1029/2001JD001236.

Hagan, M. E., and R. G. Roble (2001), Modelling diurnal tidal variability with the NCAR TIME-GCM, *J. Geophys. Res.*, *106*, 24,869–24,882.

Hagan, M. E., J. M. Forbes, and F. Vial (1995), On modeling migrating solar tides, *Geophys. Res. Lett.*, *22*, 893–896.

Hagan, M. E., J. L. Chang, and S. K. Avery (1997), Global-Scale Wave Model estimates of nonmigrating tidal effects, *J. Geophys. Res.*, *102*, 16,439–16,452.

Hagan, M. E., R. G. Roble, and J. Hackney (2001), Migrating thermospheric tides, *J. Geophys. Res.*, *106*, 12,739–12,752.

Hamilton, K. (1981), Latent heat release as a possible forcing mechanism for atmospheric tides, *Mon. Wea. Rev.*, *109*, 3–17.

Hays, P. B., et al. (1994), Observations of the diurnal tide from space, *J. Atmos. Sci.*, *51*, 3077–3093.

Hitchman, M. H., and C. B. Leovy (1985), Diurnal tide in the equatorial middle atmosphere as seen in LIMS temperatures, *J. Atmos. Sci.*, *42*, 557–561.

Huang, F. T., and C. A. Reber (2003), Seasonal behavior of the semidiurnal and diurnal tides, and mean flows at 95 km, based on measurements from the High Resolution Doppler Imager (HRDI) on the Upper Atmosphere Reasearch Satellite (UARS), *J. Geophys. Res.*, *108*, 4360, doi:10.1029/2002JD003189.

Huang, F. T., and C. A. Reber (2004), Nonmigrating semidiurnal and diurnal tides at 95 km based on wind measurements from the High Resolution Doppler Imager on UARS, *J. Geophys. Res.*, *109*, D10,110, doi:10.1029/2003JD004442.

Huang, F. T., H. G. Mayr, C. A. Reber, T. Killeen, J. Russell, M. Mlynczak, W. Skinner, and J. Mengel (2006), Diurnal variations of temperature and winds inferred from TIMED and UARS measurements, *J. Geophys. Res.*, *111*, A10S04, doi:10.1029/2005JA011426.

Kato, S., T. Tsuda, and F. Watanabe (1982), Thermal excitation of nonmigrating tides, *J. Atmos. Sol.-Terr. Phys.*, *44*, 131–146.

Khattatov, B. V., M. A. Geller, V. A. Yudin, and P. B. Hays (1997), Diurnal migrating tide as seen by the high-resolution Doppler imager/UARS. 2. Monthly mean global zonal and vertical velocities, pressure, temperature, and inferred dissipation, *J. Geophys. Res.*, *102*, 4423–4435.

Kinnison, D. E., et al. (2007), Sensivity of chemical tracers to meteorological parameters in the MOZART-3 chemical transport model, *J. Geophys. Res.*, in press.

Kodera, K., and Y. Kuroda (2002), Dynamical response to the solar cycle, *J. Geophys. Res.*, *107*, 4749, doi:10.1029/2002JD002224.

Lieberman, R. S. (1991), Nonmigrating diurnal tides in the equatorial middle atmosphere, *J. Atmos. Sci.*, *48*, 1112–1123.

Lieberman, R. S., and C. Leovy (1995), A numerical model of nonmigrating diurnal tides between the surface and 65 km, *J. Atmos. Sci.*, *52*, 389–409.

Lieberman, R. S., J. Oberheide, M. E. Hagan, E. E. Remsberg, and L. L. Gordley (2004), Variability of diurnal tides and planetary waves during November 1978–May 1979, *J. Atmos. Sol.-Terr. Phys.*, *66*, 517–528.

Luo, A. H. M. Y., and C. Meek (2002), Global distributions of diurnal and semidiurnal tides: observations from HRDI-UARS of the MLT region, *Ann. Geophys.*, *20*, 1877–

636 1890.

637 Manson, A., et al. (1999), Seasonal variations of the semi-diurnal and diurnal tides in the
638 MLT: Multi-year MF radar observations from 2 to 70N, and the GSWM tidal model,
639 *J. Atmos. Sol.-Terr. Phys.*, *61*, 809–828.

640 Manson, A. H., C. Meek, M. Hagan, X. Zhang, and Y. Luo (2004), Global distributions of
641 diurnal and semidiurnal tides: observations from HRDI-UARS of the MLT region and
642 comparisons with GSWM-02 (migrating, nonmigrating components), *Ann. Geophys.*,
643 *22*, 1529–1548.

644 Manzini, E., M. A. Giorgetta, M. Esch, L. Kornblueh, and E. Roeckner (2006), The
645 influence of sea surface temperatures on the northern winter stratosphere: Ensemble
646 simulations with the MAECHAM5 model, *J. Climate*, *19*, 3863–3881.

647 Matthes, K., U. Langematz, L. L. Gray, K. Kodera, and K. Labitzke (2004), Improved
648 11–year solar signal in the Freie Universität Berlin Climate Middle Atmosphere Model
649 (FUB–CMAM), *J. Geophys. Res.*, *109*, D06,101, doi:10.1029/2003JD004012.

650 McLandress, C. (2002a), The seasonal variation of the propagating diurnal tide in the
651 mesosphere and lower thermodphere. Part I: The role of gravity waves and planetary
652 waves, *J. Atmos. Sci.*, *59*, 893–906.

653 McLandress, C. (2002b), The seasonal variation of the propagating diurnal tide in the
654 mesosphere and lower thermodphere. Part II: The role of tidal heating and zonal mean
655 winds, *J. Atmos. Sci.*, *59*, 907–922.

656 McLandress, C., G. G. Shepherd, and B. H. Solheim (1996), Satellite observations of ther-
657 mospheric tides: Results from the Wind Imaging Interferometer on UARS, *J. Geophys.*
658 *Res.*, *101*, 4093–4114.

659 Miyahara, S., Y. Miyoshi, and K. Yamashita (1999), Variations of migrating and nonmi-
660 grating tides simulated by the middle atmosphere circulation model at Kyushu Univer-
661 sity, *Adv. Space Res.*, *24*, 1549–1558.

662 Oberheide, J., and O. A. Gusev (2002), Observation of migrating and nonmigrating
663 diurnal tides in the equatorial lower thermosphere, *Geophys. Res. Lett.*, *29*, 2167,
664 doi:10.1029/2002GL016231.

665 Oberheide, J., M. E. Hagan, W. E. Ward, M. Riese, and D. Offermann (2000), Mod-
666 elling the diurnal tide for the Cryogenic Infrared Spectrometers and Telescopes for the
667 Atmosphere (CRISTA) 1 time period, *J. Geophys. Res.*, *105*, 24,917–24,929.

668 Oberheide, J., Q. Wu, D. A. Ortland, T. L. Killeen, M. E. Hagan, R. G. Roble, R. J.
669 Niciejewski, and W. R. Skinner (2005), Non-migrating diurnal tides as measured by the
670 TIMED Doppler interferometer: preliminary results, *Adv. Space Res.*, *35*, 1911–1917,
671 doi:10.1016/j.asr.2005.01.063.

672 Oberheide, J., Q. Wu, T. L. Killeen, M. E. Hagan, and R. G. Roble (2006), Diurnal non-
673 migrating tides from TIMED Doppler Interferometer wind data: monthly climatologies
674 and seasonal variations, *J. Geophys. Res.*, *111*, A10S03, doi:10.1029/2005JA011491.

675 Ortland, D. A. (2005a), Generalized Hough modes: The structure of damped globals-scale
676 waves propagating on a mean flow with horizontal and vertical shear, *J. Atmos. Sci.*,
677 *62*, 2674–2683.

678 Ortland, D. A. (2005b), A study of the global structure of the migrating diurnal tide using
679 generalized Hough modes, *J. Atmos. Sci.*, *62*, 2684–2702.

680 Ortland, D. A., and M. Alexander (2006), Gravity wave influence on the global structure
681 of the diurnal tide in the mesosphere and lower thermosphere, *J. Geophys. Res.*, *111*,

682 A10S10, doi:10.1029/2005JA011467.

683 Schmidt, H., G. P. Brasseur, E. Manzini, M. A. Giorgetta, T. Diehl, V. I. Fomichev,
684 D. Kinnison, D. Marsh, and S. Walters (2006), The HAMMONIA chemistry climate
685 model: Sensitivity of the mesopause region to the 11-year solar cycle and CO_2 doubling,
686 *J. Climate*, *19*, 3903–3931.

687 Shepherd, M. G., W. E. Ward, B. Prawirosoehardjo, R. G. Roble, S. P. Zhang, and
688 D. Y. Wang (1999), Planetary scale and tidal perturbations in meospheric temperatures
689 observed by WINDII, *Earth Planets Space*, *51*, 593–610.

690 Talaat, E. R., and R. S. Lieberman (1999), Nonmigrating diurnal tides in mesospheric
691 and lower-thermospheric winds and temperatures, *J. Atmos. Sci.*, *56*, 4073–4087.

692 Tsuda, T., and S. Kato (1989), Diurnal non-migrating tides excited by a differential
693 heating due to land-sea distribution, *J. Met. Soc. Japan*, *67*, 43–55.

694 Tsuda, T., et al. (1999), Coordinated radar observations of atmospheric diurnal tides in
695 equatorial regions, *Earth Planets Space*, *51*, 579–592.

696 Vial, F., and J. M. Forbes (1989), Recent progress in tidal modelling, *J. Atmos. Terr.*
697 *Phys.*, *51*, 663–671.

698 Vincent, R. A., T. Tsuda, and S. Kato (1988), A comparative study of mesospheric solar
699 tides observed at Adelaide and Kyoto, *J. Geophys. Res.*, *93*, 699–708.

700 Vincent, R. A., S. Kovalam, D. C. Fritts, and J. R. Isler (1998), Long-term MF radar
701 observations of solar tides in the low-latitude mesosphere: Interannual variability and
702 comparisons with the GSWM, *J. Geophys. Res.*, *103*, 8667–8683.

703 Wallace, J. M., and R. F. Tadd (1974), Some further results concerning the vertical
704 structure of atmospheric tidal motions within the lowest 30 km, *Mon. Wea. Rev.*, *102*,

795–803.

Wu, D. L., C. McLandress, E. F. Fishbein, W. G. Read, J. W. Waters, and L. Froidevaux (1998), Equatorial diurnal variations observed in UARS MLS temperature during 1991–1994 and simulated by the CMAM, *J. Geophys. Res.*, *103*, 8909–8917.

Wu, Q., T. L. Killeen, D. A. Ortland, S. C. Solomon, R. D. Gablehouse, R. M. Johnson, W. R. Skinner, R. J. Niciejewski, and S. J. Franke (2006), TIMED Doppler interferometer (TIDI) observations of migrating diurnal and semidiurnal tides, *J. Atmos. Sol.-Terr. Phys.*, *68*, 408–417.

Yagai, L. (1989), Nonmigrating thermal tides detected in the data analysis and a general circulation model simulation, *J. Geophys. Res.*, *94*, 6341–6356.

Zhang, S. P. P., and G. G. Shepherd (2005), Variations of the mean winds and diurnal tides in the meospshere and lower thermosphere observed by WINDII from 1992 to 1996, *Geophys. Res. Lett*, *32*, L14,111, doi:10.1029/2005GL023293.

Zhang, X., J. M. Forbes, M. E. Hagan, J. M. R. III, S. E. Palo, C. J. Mertens, and M. G. Mlynczak (2006), Monthly tidal temperatures 20–120 km from TIMED/SABER, *J. Geophys. Res.*, *111*, A10S08, doi:10.1029/2005JA011504.

Zhu, X., J.-H. Yee, E. R. Talaat, M. Mlynczak, L. Gordley, C. Mertens, and J. M. R. III (2006), An algorithm for extracting zonal mean and migrating tidal fields in the middle atmosphere from satellite measurements: applications to TIMED/SABER-measured temperature and tidal modelling, *J. Geophys. Res.*, *110*, D02,105, doi:10.1029/2005JD004996.

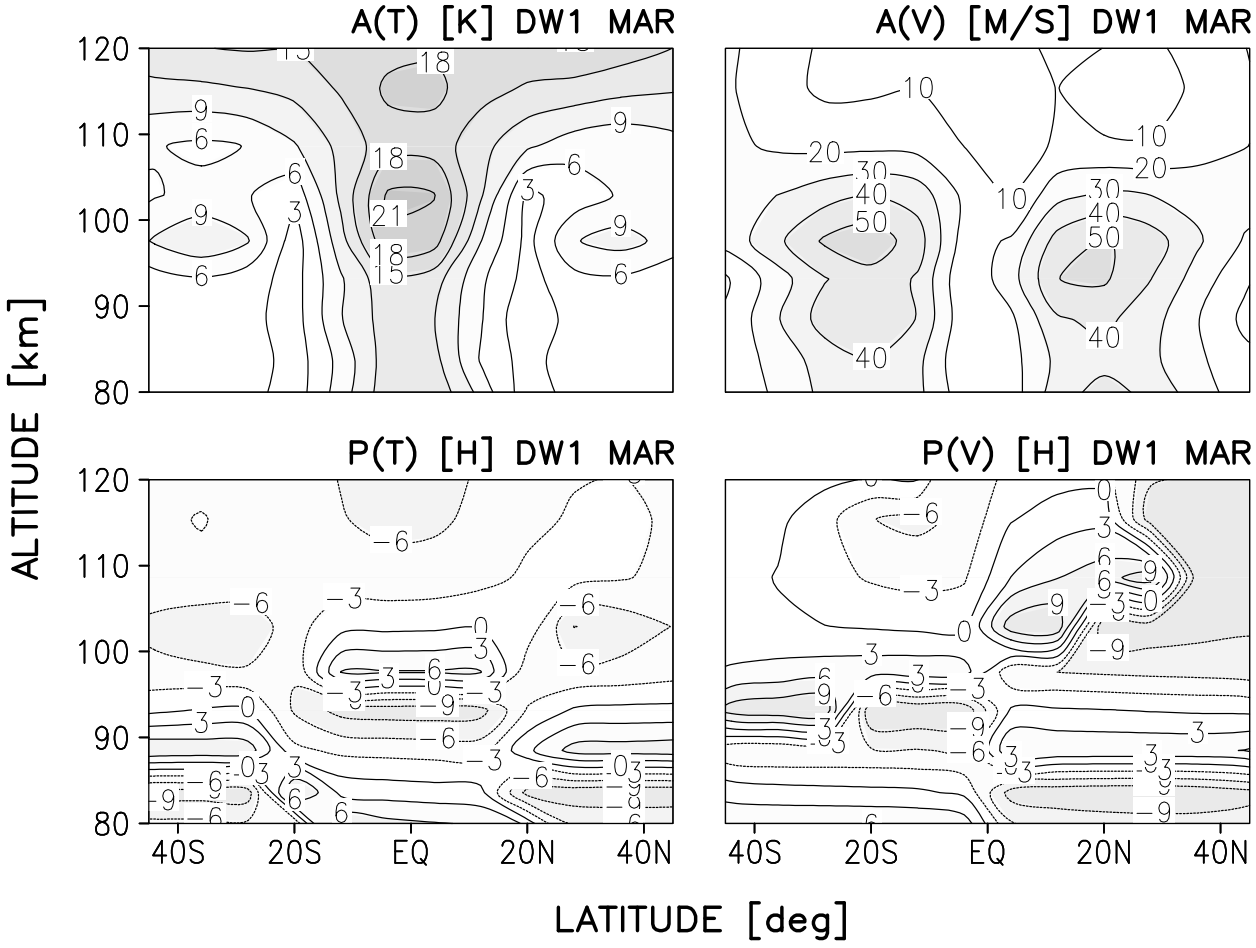

Figure 1. The March amplitudes (top row) and phases (bottom) of the migrating diurnal tide in the temperature (left column) and meridional south-north wind (right) from the HAMMONIA model. The amplitudes are in units of K and m/s, respectively. The phases indicate the local solar time, in h, at which the maximum value is attained.

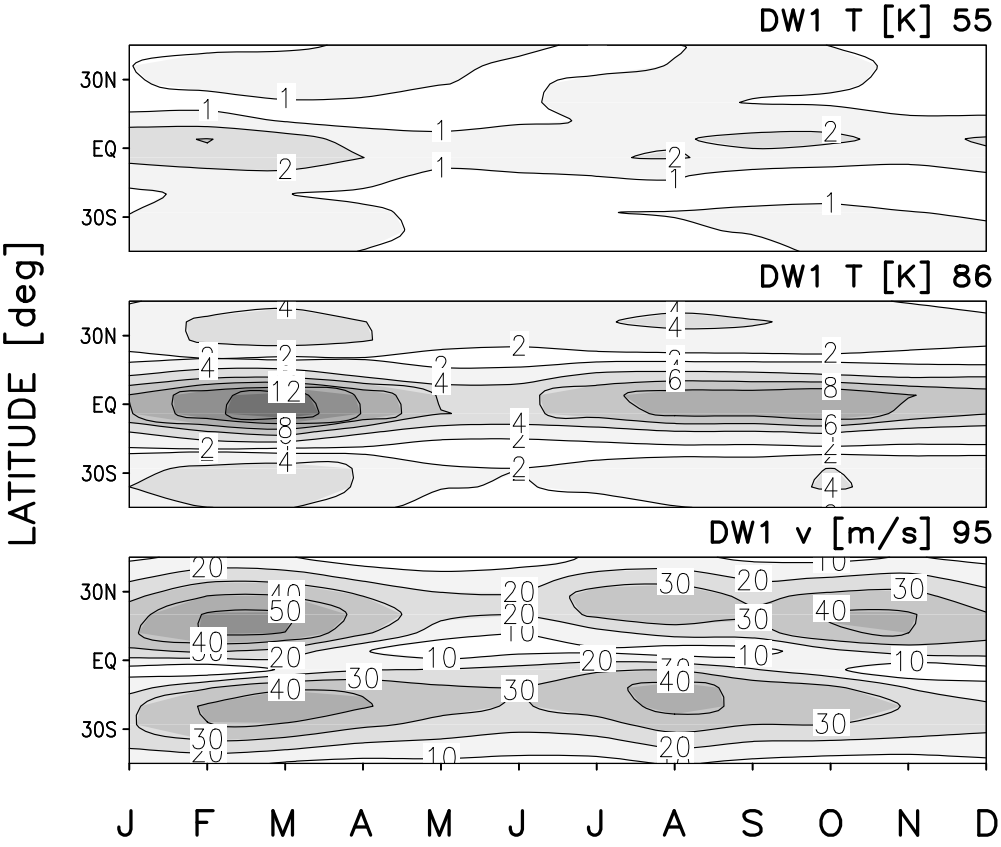

Figure 2. The seasonal dependence of the amplitudes of the tropical migrating diurnal tide in the temperature at 55km (top panel) and 86km altitude (middle), and in the meridional wind at 95km (bottom) in the GCM. Units are K and m/s, respectively.

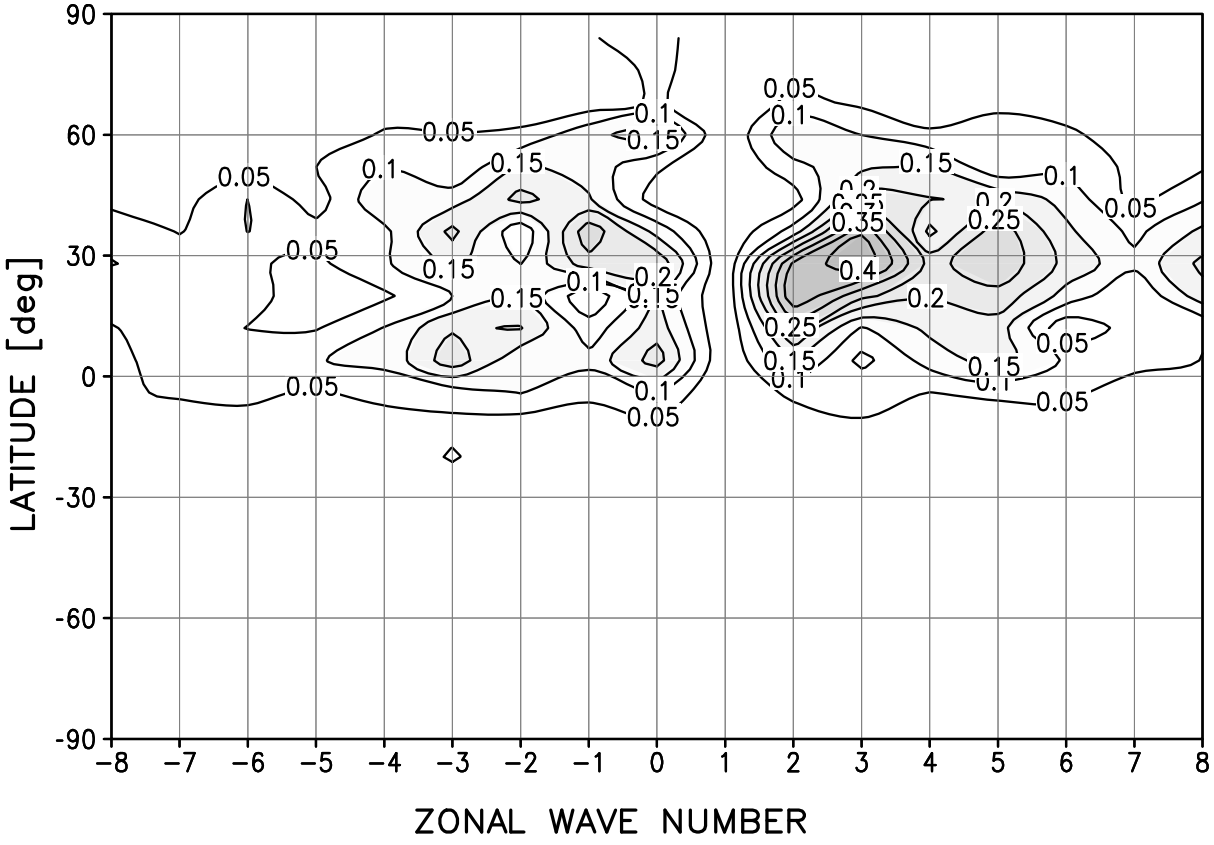

Figure 3. The amplitudes of the July nonmigrating diurnal components of the tropospheric (i.e. averaged between 0.2km and 15.2km altitude) diabatic heating of the HAMMONIA model. Negative (positive) wave numbers indicate eastward (westward) propagation. The amplitude of the migrating forcing has been set to zero. Units are in K/d.

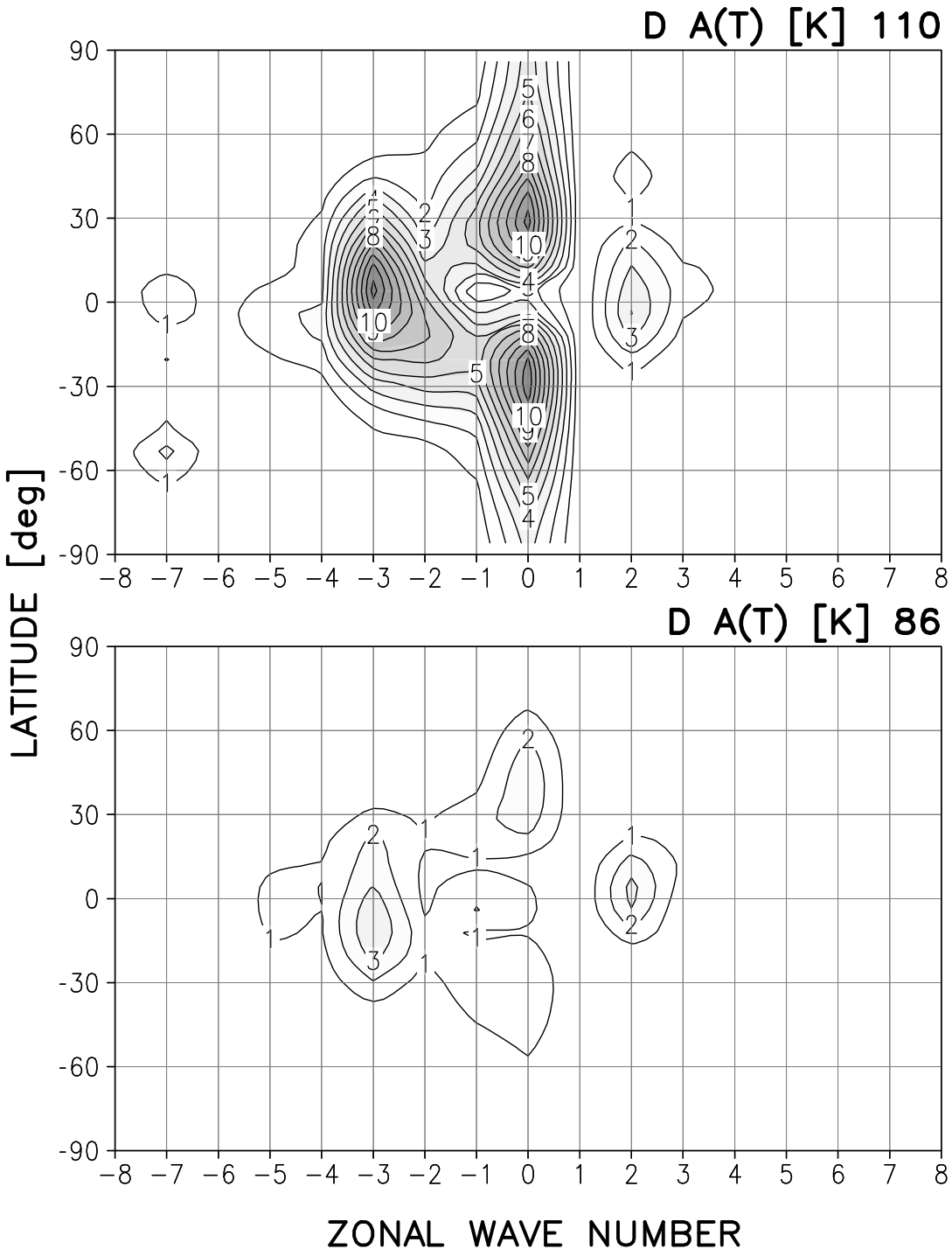

Figure 4. The amplitudes of the July nonmigrating diurnal temperature tides of the HAMMONIA model at 110km (top panel) and 86km (bottom) altitude. Negative (positive) wave numbers indicate eastward (westward) propagation. The amplitude of the migrating tide has been set to zero. Units are in K.

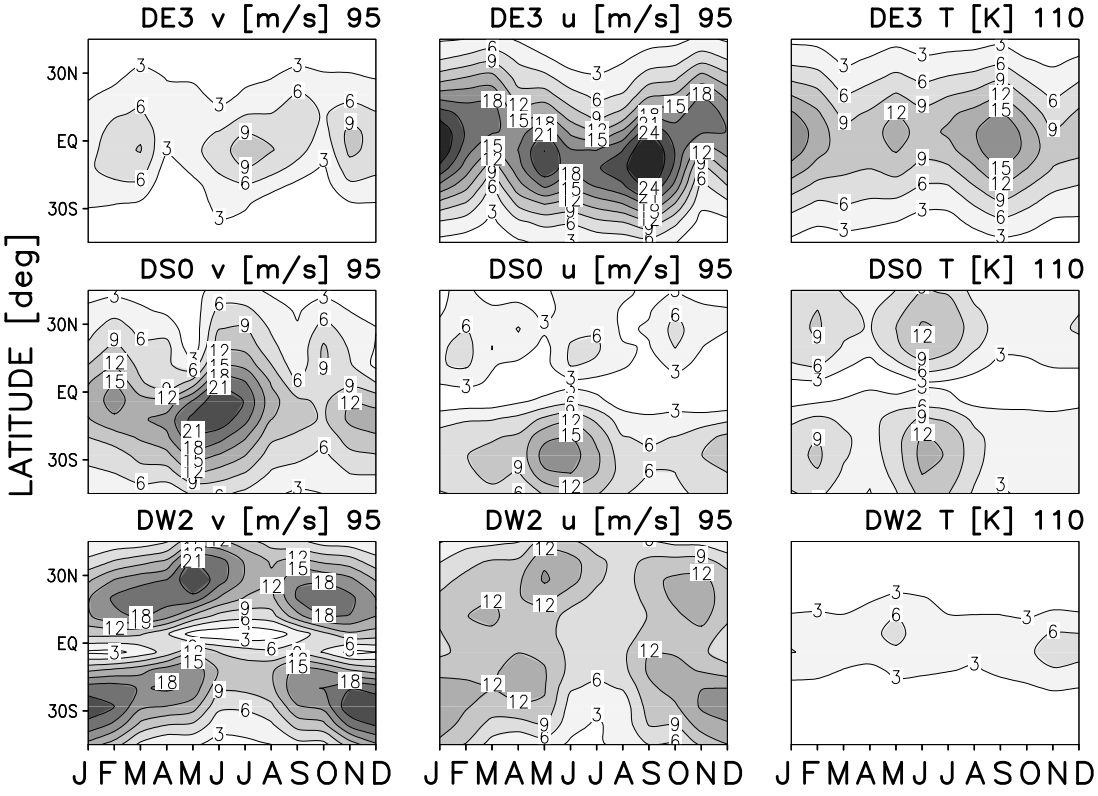

Figure 5. Seasonal cycle of the amplitudes of various nonmigrating diurnal components in HAMMONIA. Shown are DE3 (top row), DS0 (middle), and DW2 (bottom) in the meridional wind at 95km altitude (left column), the zonal wind at 95km (middle), and the temperature at 110km (right). Units are m/s and K, respectively.

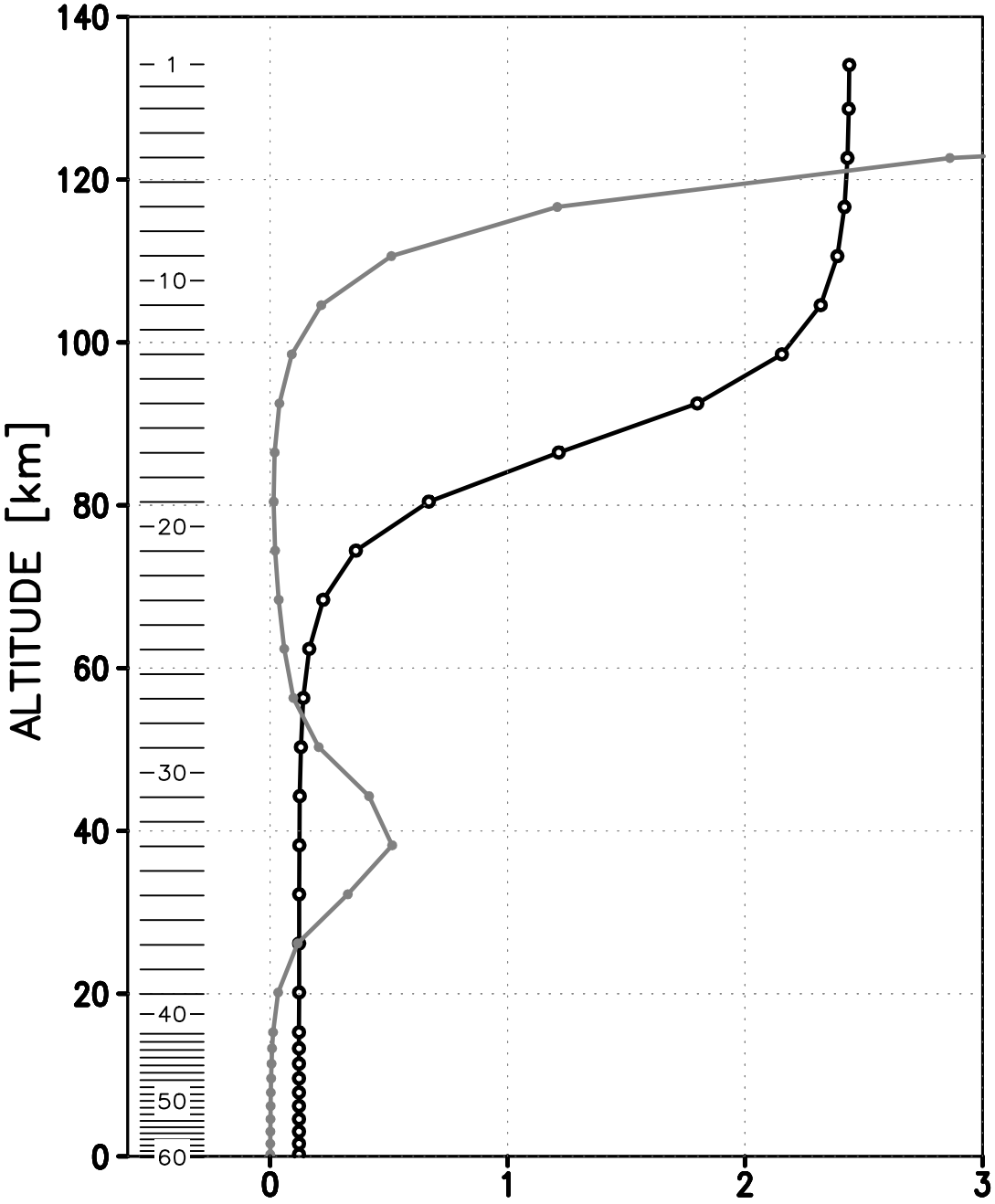

Figure 6. The vertical dependence of the Newtonian cooling (grey line, in d^{-1}) and the 4th-order horizontal diffusion (black, in $5 \cdot 10^{-20} m^4/s$) used in the linear model. Also shown is the vertical distribution of the 60 model levels, from level 1 at the top to level 60 at the bottom. In this figure logarithmic pressure altitude is used, assuming a constant scale height of 7km.

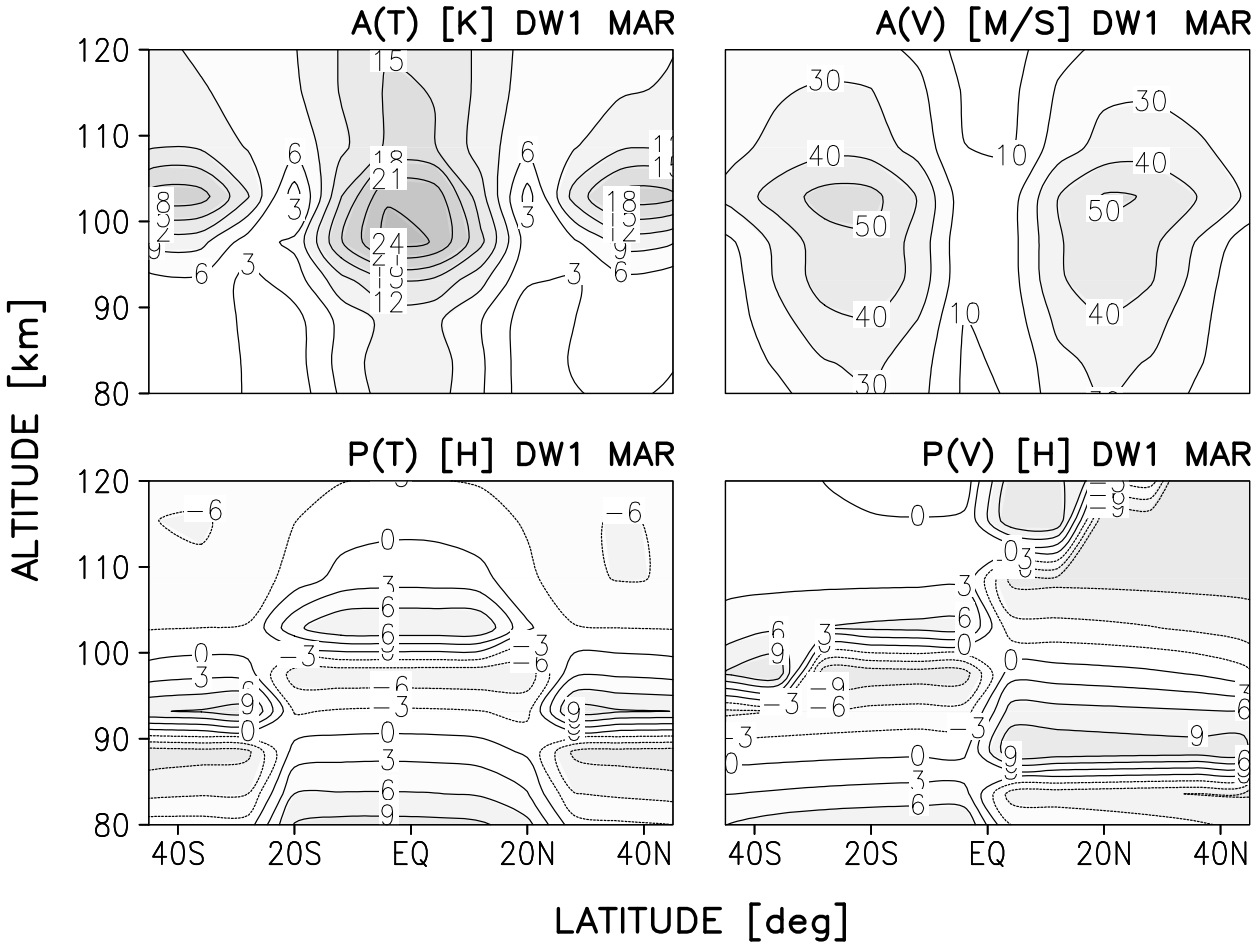

Figure 7. As Fig. 1, but for the tide calculated by the linear model using as reference atmosphere and diurnal diabatic heating the corresponding March fields from HAMMONIA.

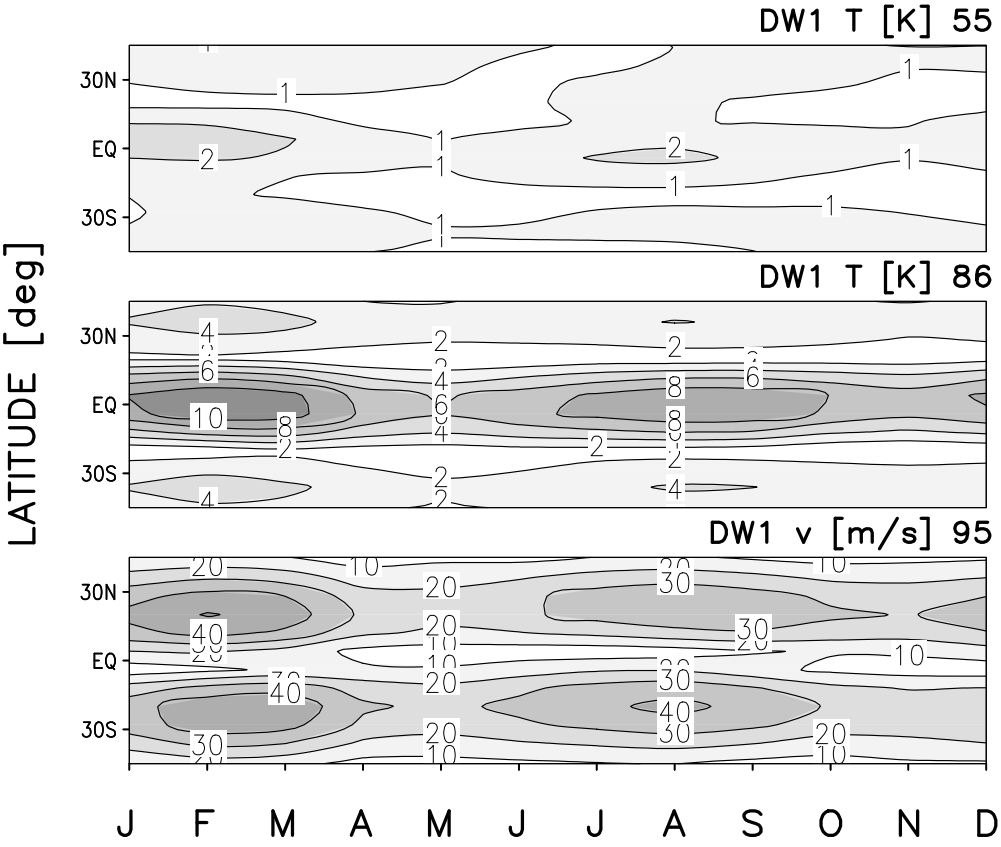

Figure 8. As Fig. 2, but showing the seasonal cycle of the migrating diurnal tide in the linear model.

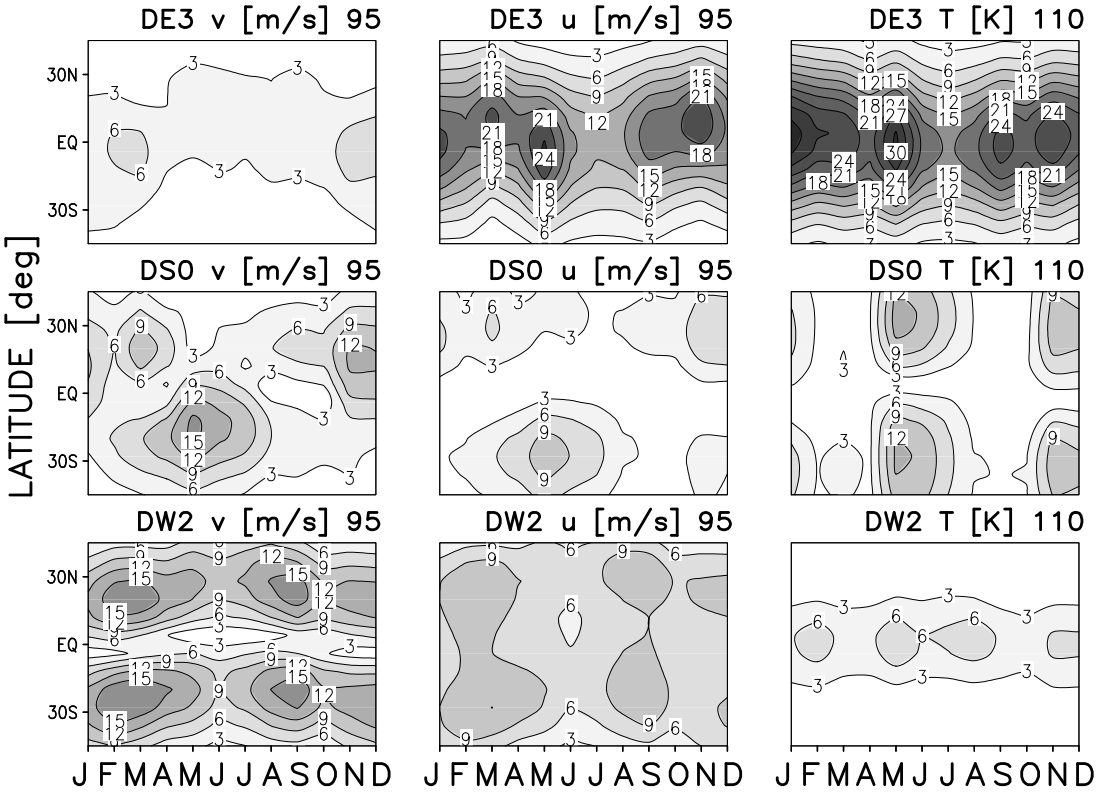

Figure 9. As Fig. 5, but showing the seasonal cycle of the amplitudes of the same nonmigrating diurnal components in the linear model.

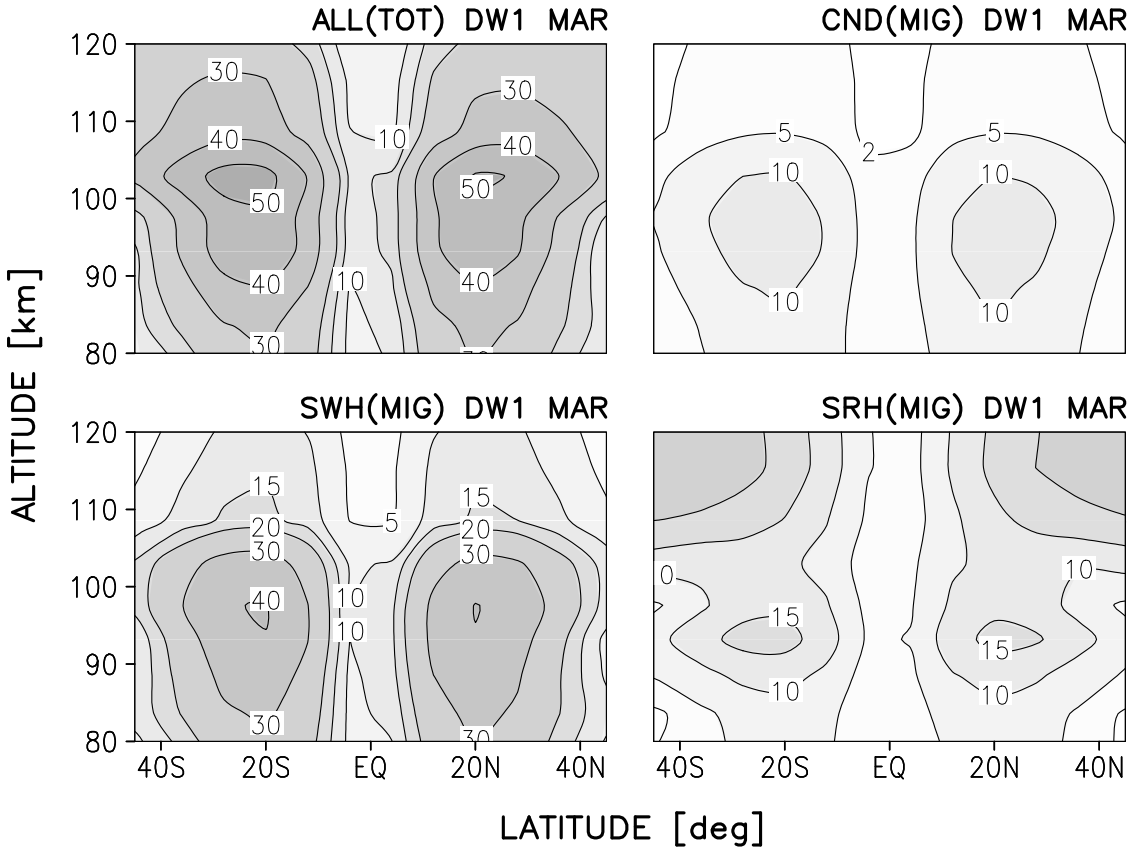

Figure 10. From the linear model, the amplitude of the March migrating diurnal tide in the meridional wind (upper left panel), and those of the three major components contributing, i.e. the response to condensation and convection (upper right), absorption of incoming solar radiation in the SW ($\lambda > 250$nm, lower left) and SR (250nm $> \lambda >$ 120nm, lower right) parts of the spectrum. Units are m/s.

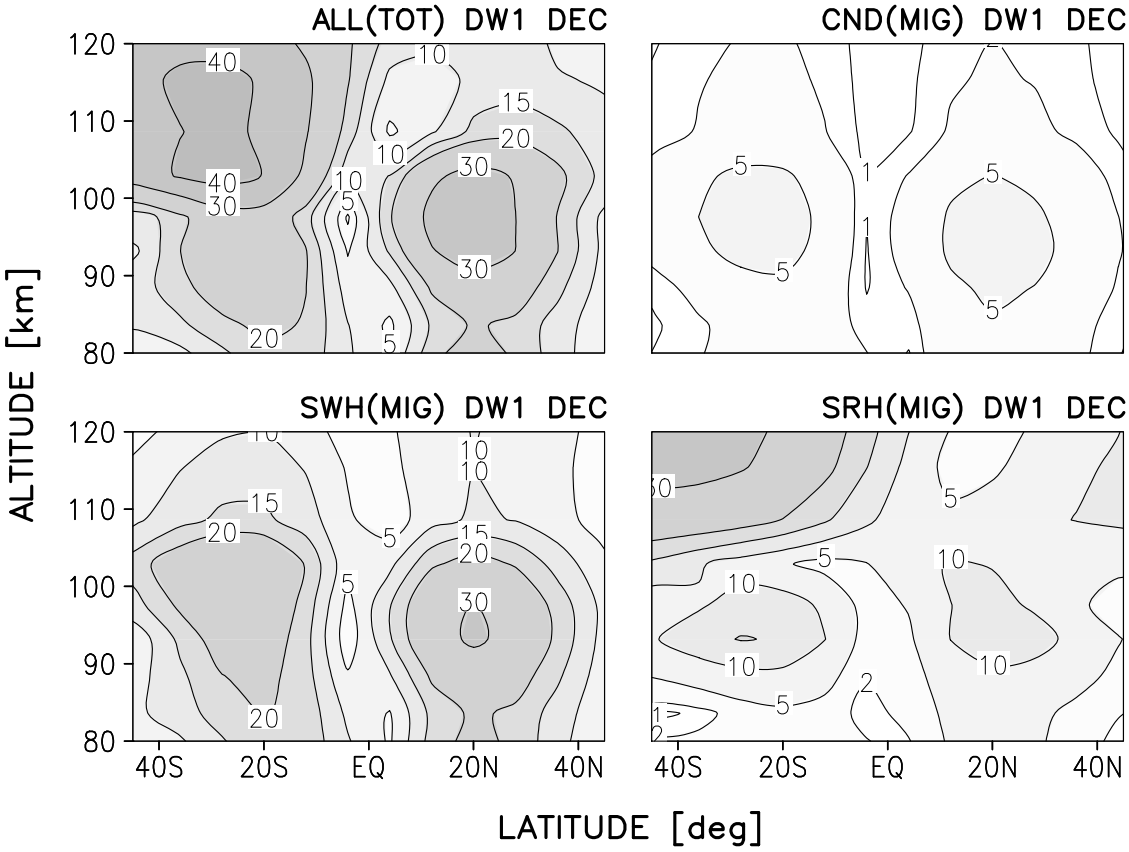

Figure 11. As Fig. 10, but for December.

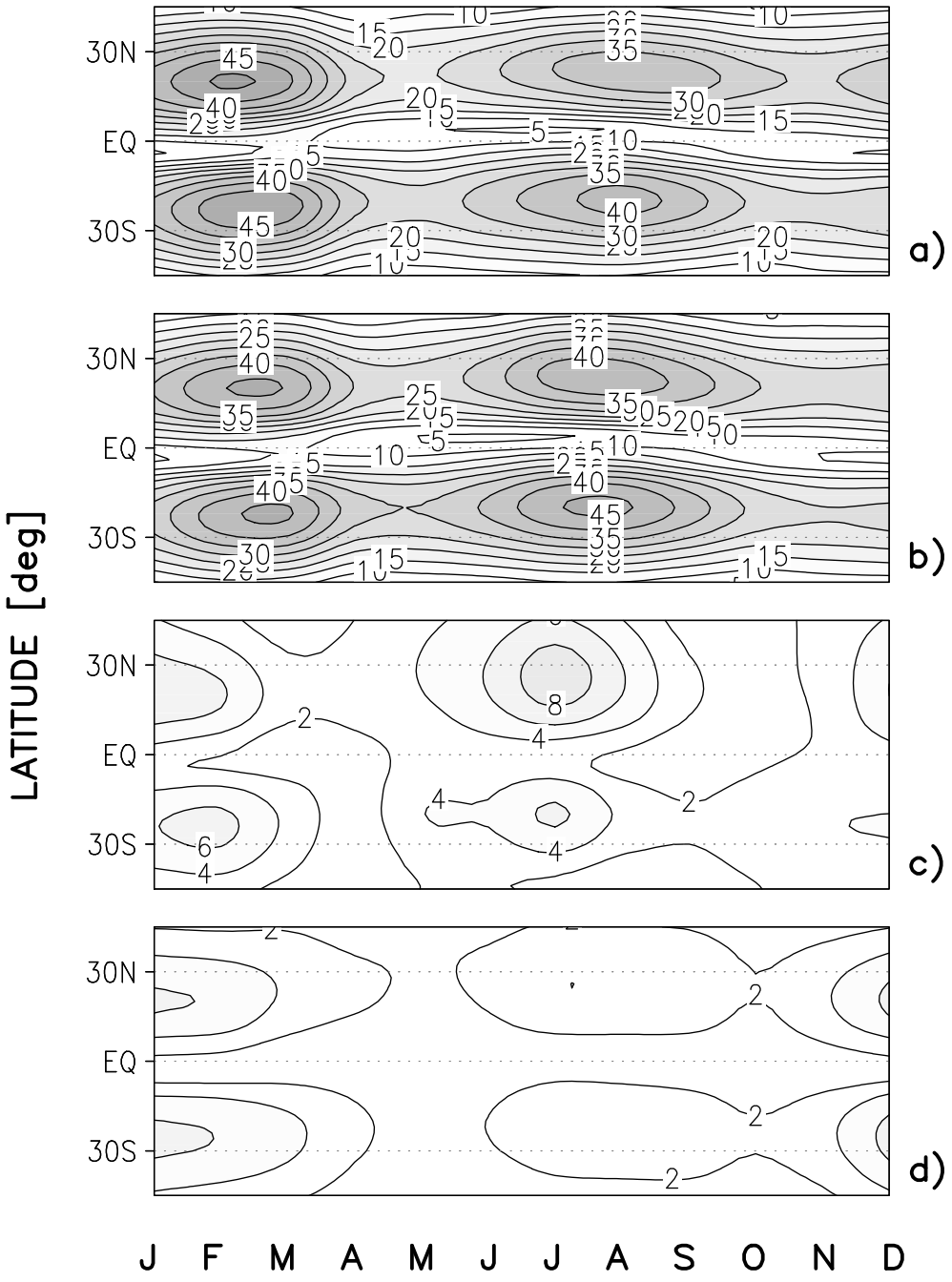

Figure 12. From the linear model, the seasonal cycle in the amplitudes of the migrating diurnal tide in the meridional wind at 95km altitude (a), the part due to variations of the background atmosphere (b), the part due to the seasonally varying part of the diurnal heat sources (c), and the corresponding contribution from the seasonal cycle of the stationary planetary waves (d). For details see the main text. Units are m/s.

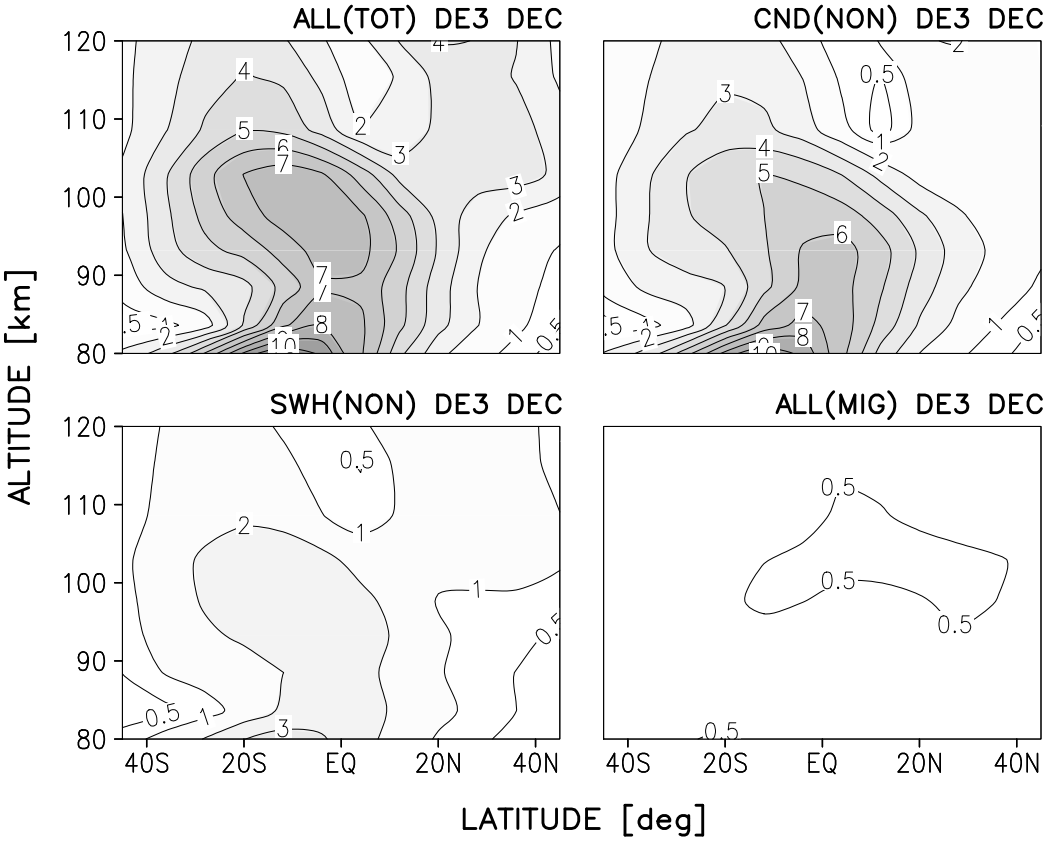

Figure 13. From the linear model, the amplitude of the December nonmigrating diurnal tide DE3 in the meridional wind (upper left panel), and that of the the two major components contributing, i.e. the response to the nonmigrating forcing by condensation and convection (upper right) and absorption of incoming solar radiation in the short-wave band (nonmigrating, lower left), and that of the response to the total migrating forcing. Units are m/s.

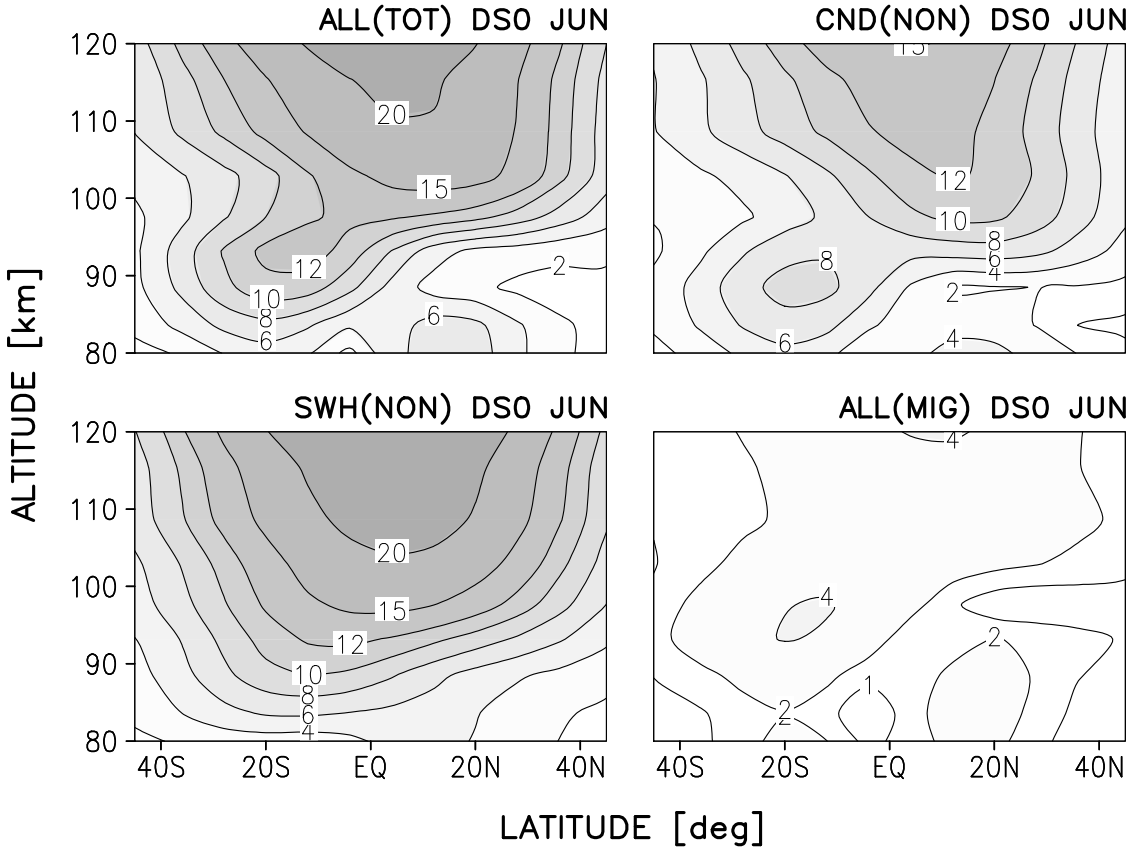

Figure 14. As Fig 13, but for the June signal in DS0.

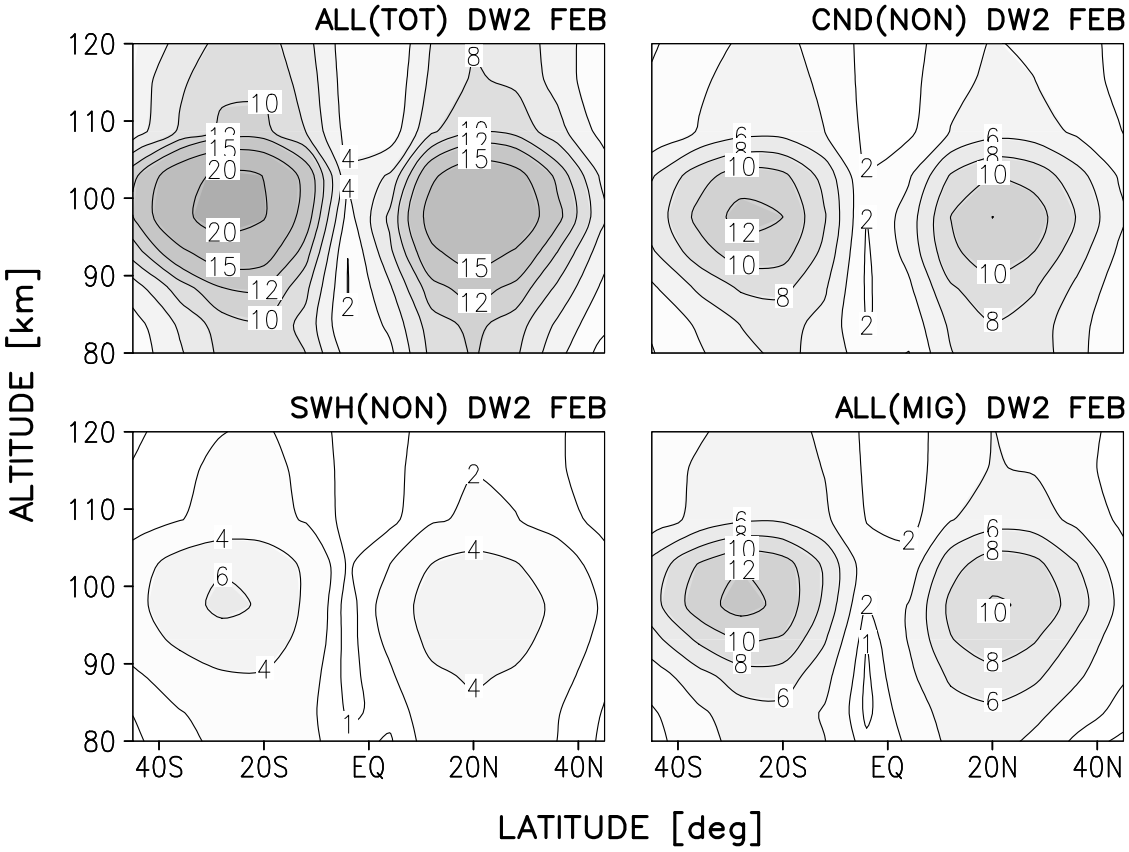

Figure 15. As Fig 13, but for the February signal in DW2.

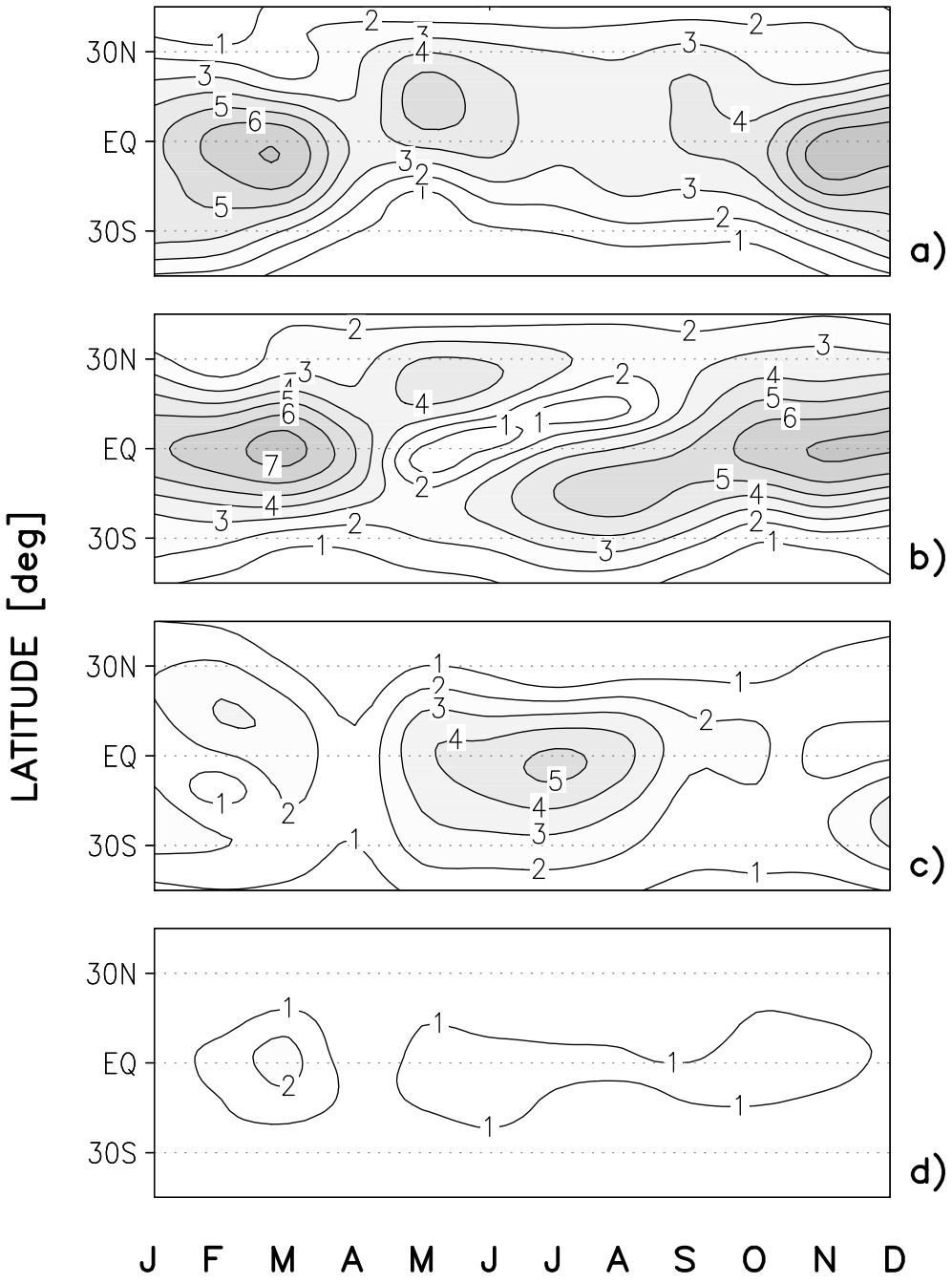

Figure 16. From the linear model, the seasonal cycle in the amplitudes of the nonmigrating component DE3 of the diurnal tide in the meridional wind at 95km altitude (a), the part due to variations of the background atmosphere (b), the part due to the seasonally varying part of the diurnal heat sources (c), and the corresponding contribution from the seasonal cycle of the stationary planetary waves (d). For details see the main text. Units are m/s.

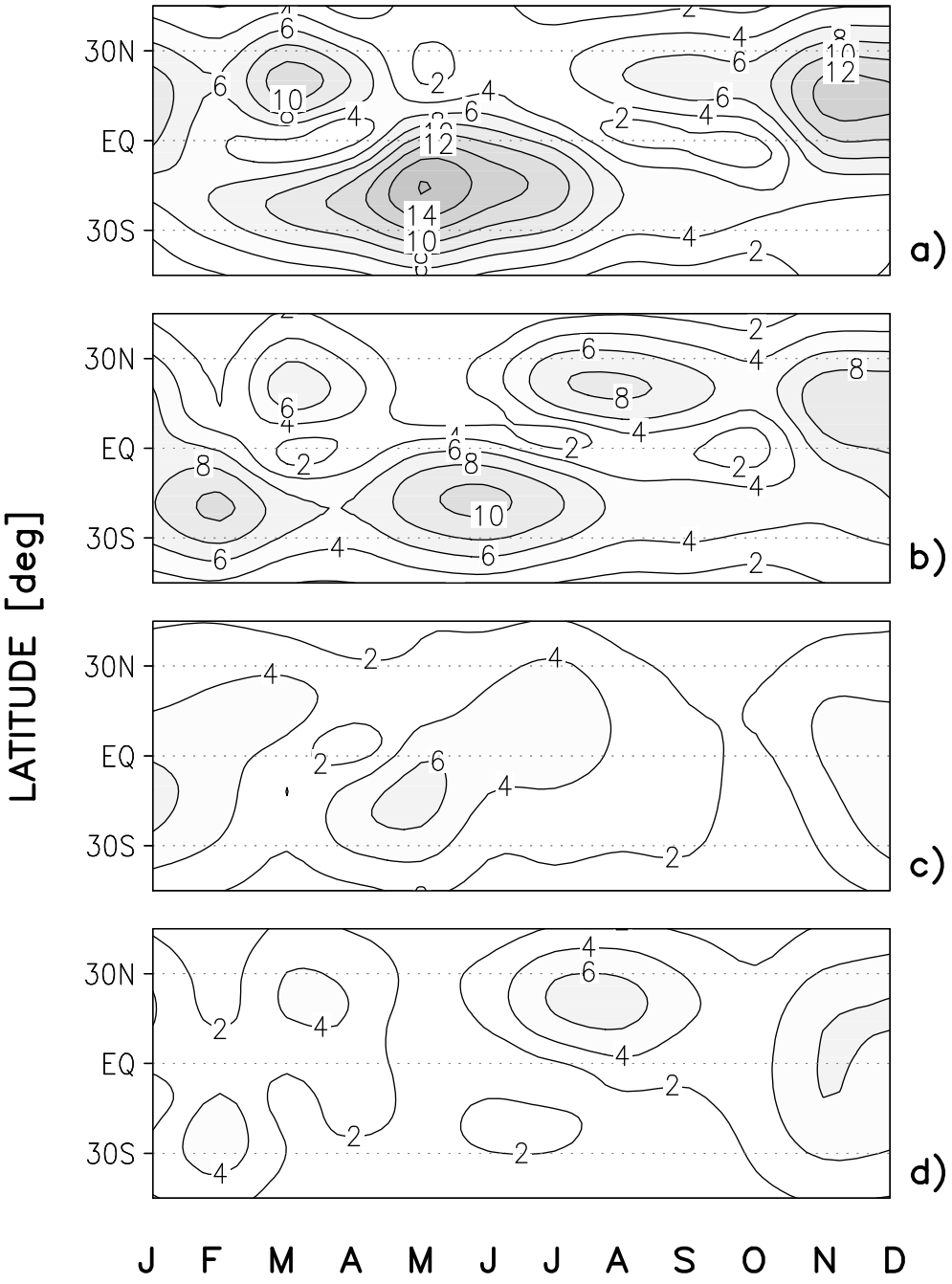

Figure 17. As Fig. 16, but for the nonmigrating component DS0.

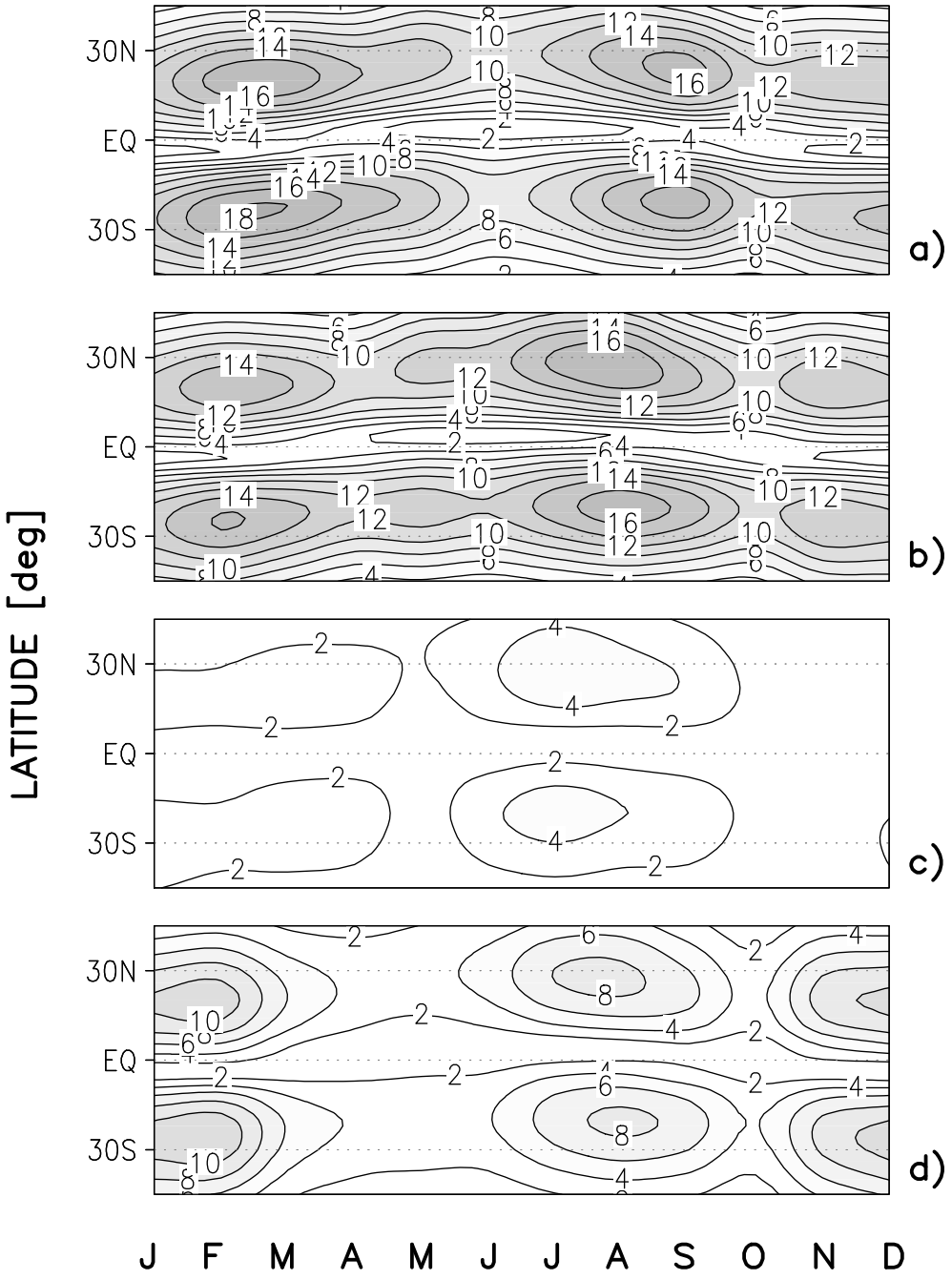

Figure 18. As Fig. 16, but for the nonmigrating component DW2.

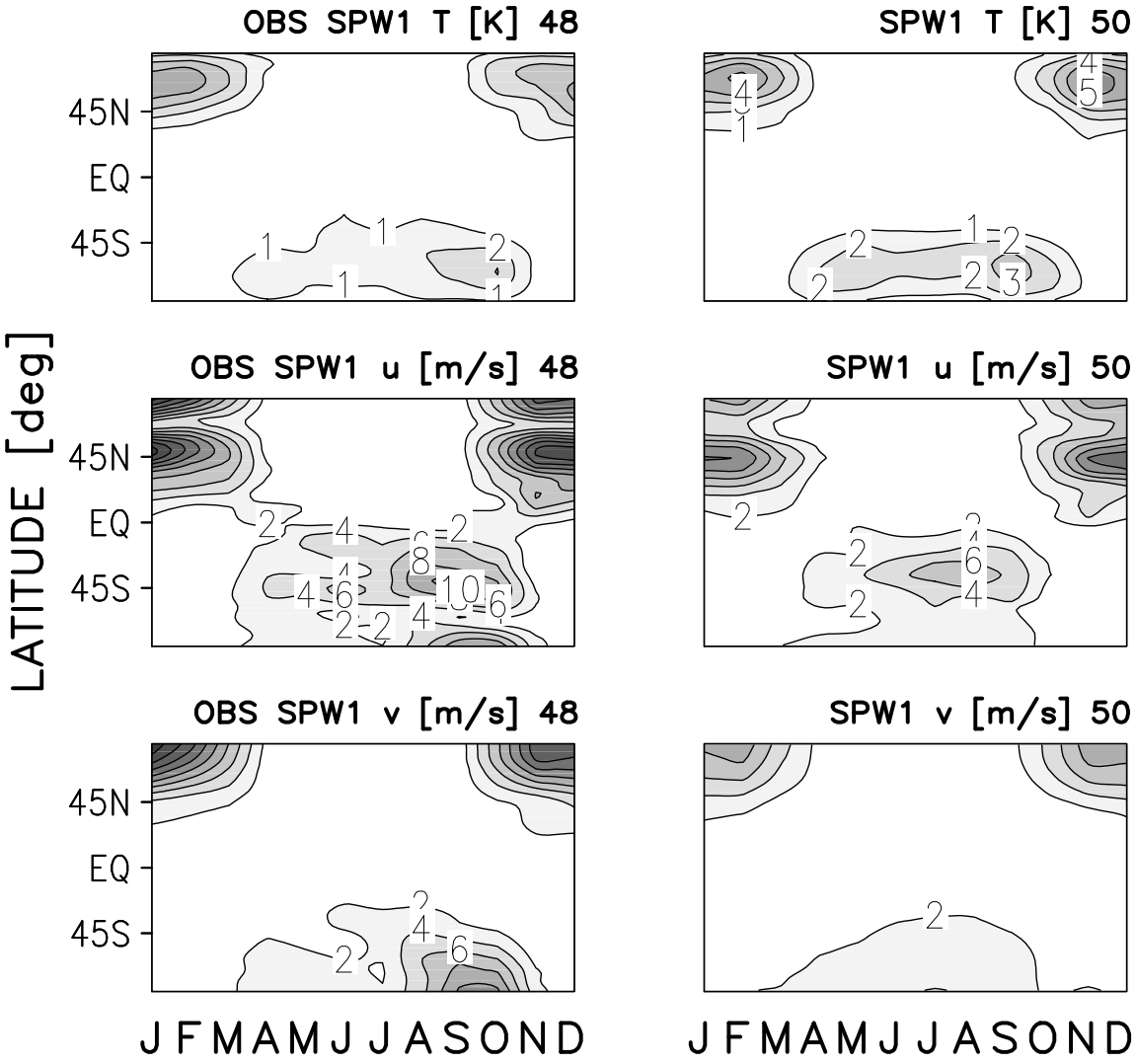

Figure 19. Comparison between the seasonal cycle in the wave at zonal wave number $s = 1$ in the monthly means of ERA-40 reanalysis data (years 1982 – 2001) at 48km altitude (left column) and HAMMONIA at 50km (right). The wave is shown in the temperature in K (top row) and in the zonal (middle) and meridional wind (bottom) in m/s.

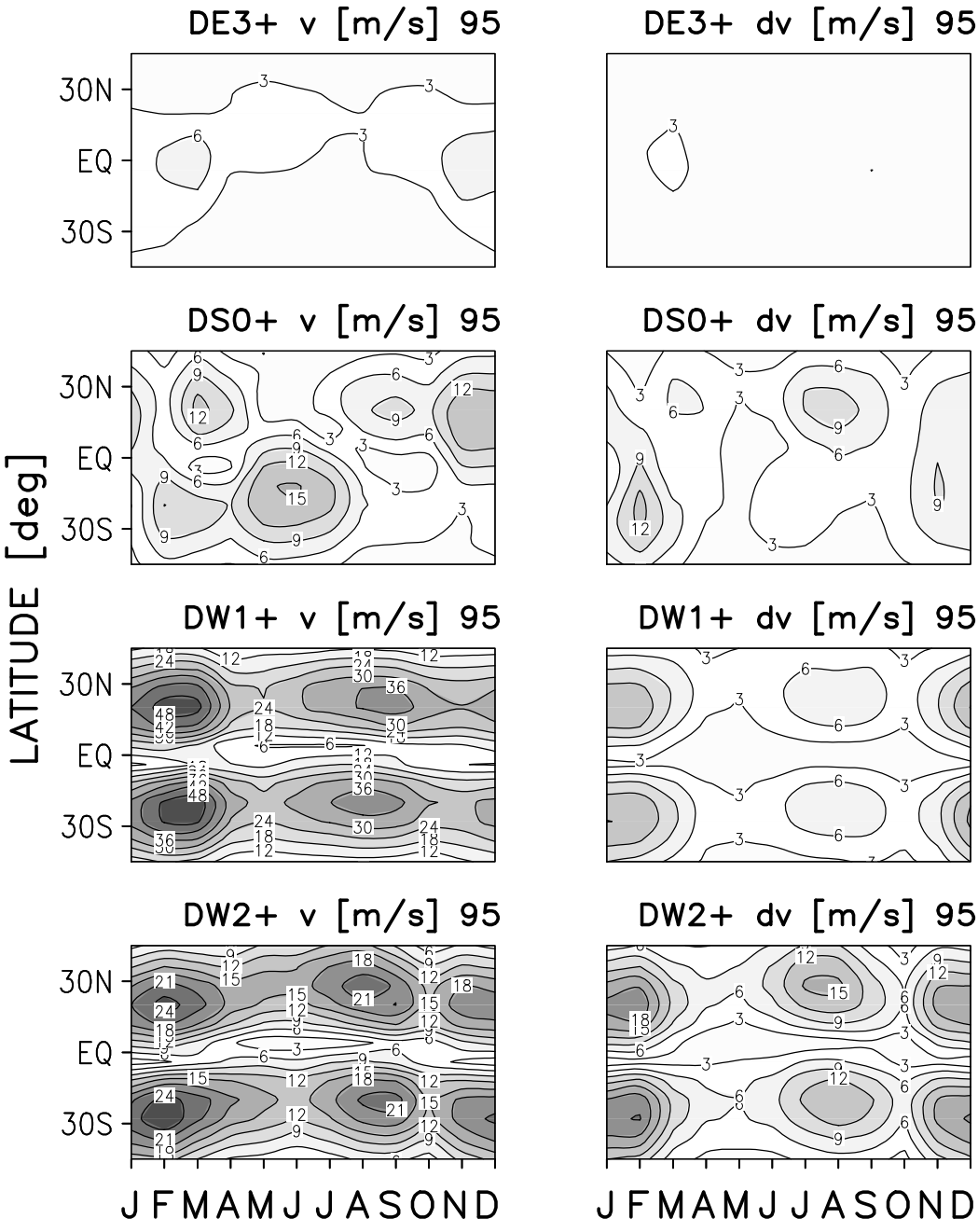

Figure 20. For the migrating tide and the three dominant nonmigrating components, the seasonal cycle in the meridional-wind amplitude at 95km altitude, obtained by the linear model with a planetary-wave amplitude in the background which is twice the GCM value in the horizontal wind, but the same in the temperature. The left column shows the total signal. The right column shows the corresponding planetary-wave impact.

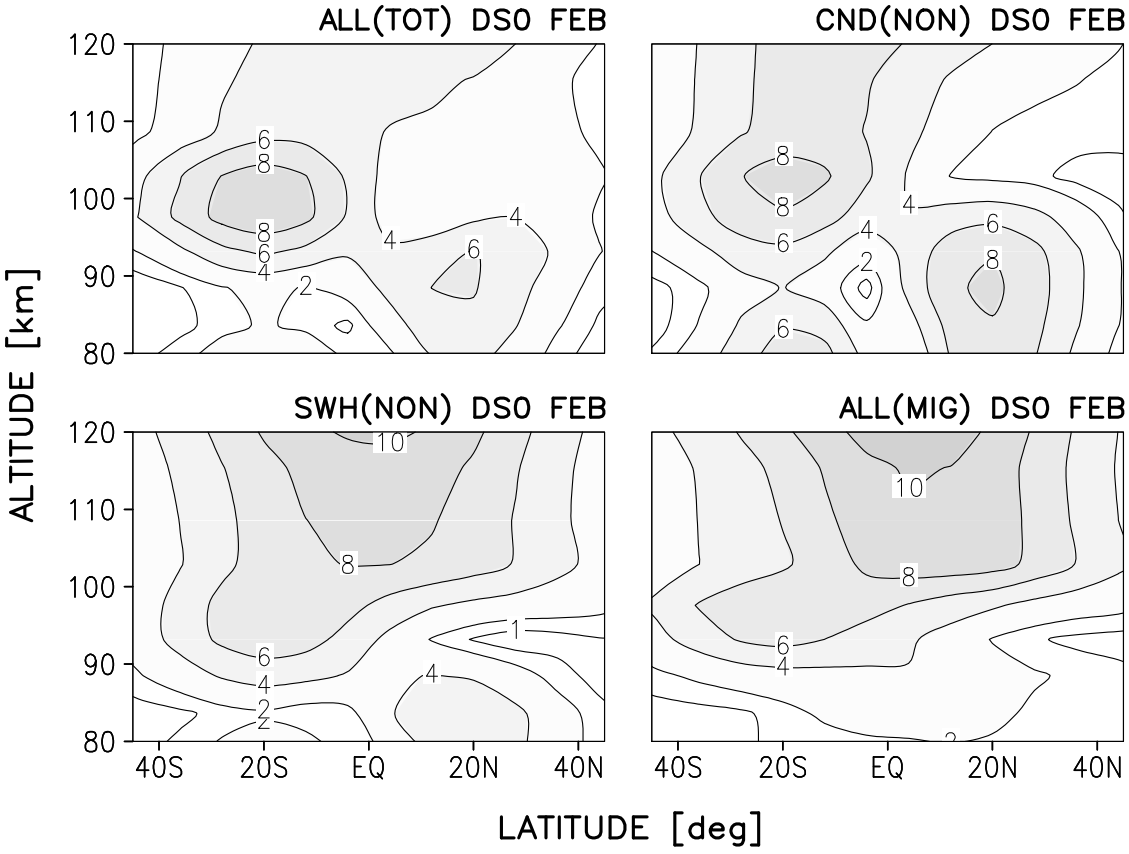

Figure 21. From the linear model, the amplitude of the February nonmigrating diurnal tide DS0 in the meridional wind (upper left panel), and that of the three major components contributing, i.e. the response to the nonmigrating forcing by condensation and convection (upper right), absorption of incoming solar radiation in the short-wave band (nonmigrating lower left), and the response to the total migrating forcing. Units are m/s.